CHEMISTRY
A EUROPEAN JOURNAL

DOI: 10.1002/chem.200601651

Shaping and Enforcing Coordination Spheres: The Implications of C_3 and C_1 Chirality in the Coordination Chemistry of 1,1,1-Tris(oxazolinyl)ethane ("Trisox")

Lutz H. Gade,*[a] Guido Marconi,[a] Clémence Dro,[b] Benjamin D. Ward,[a] Macarena Poyatos,[b] Stéphane Bellemin-Laponnaz,*[b] Hubert Wadepohl,[a] Lorenzo Sorace,[c] and Giordano Poneti[c]

Dedicated to Professor Walter Siebert on the occasion of his 70th birthday

Abstract: A key feature of tris(oxazolinyl)ethane ("trisox") ligands, which have shown broad scope in asymmetric catalysis, is the orientation and steric demand of their oxazoline substituents. This, along with the modularity of their synthesis determines their coordination chemistry. The possibility to combine oxazolines, in which the stereogenic centers adjacent to the N-donor atoms have different absolute configuration, whilst retaining their ability to coordinate as *tripodal* ligands, has been demonstrated by the synthesis of the enantiomerically pure C_3-symmetric *i*Pr-trisox(*S*,*S*,*S*) and C_1-symmetric *i*Pr-trisox(*S*,*S*,*R*) and their reaction with $[Mo(CO)_3(NCMe)_3]$ yielding [Mo{*i*Pr-trisox(*S*,*S*,*S*)}$(CO)_3$] (**1a**) and [Mo{*i*Pr-trisox(*S*,*S*,*R*)}$(CO)_3$] (**1b**), respectively. The non-autocomplementarity of two homochiral trisox ligands at one metal center has been demonstrated by reaction of *rac*-C_3 *i*Pr-trisox with one equivalent of $[Co(ClO_4)_2]\cdot 6H_2O$, giving the centrosymmetric heterochiral complex $[Co(i\text{Pr-trisox})_2](ClO_4)_2$ (**3**), whereas an analogous reaction with the enantiopure ligand yielded a mixture of Co^{II} complexes, which is characterized by the total absence of a $[(trisox)_2Co]^{+/2+}$ ion. The scope of the trisox ligand in terms of facial coordination to both early and late transition metals was demonstrated by the synthesis and structural characterization of the mononuclear complexes $[ScCl_3(i\text{Pr-trisox})]$ (**4**), $[Fe(t\text{Bu-trisox})(NCMe)_3](BF_4)_2$ (**5**), and $[Ru(\eta^6\text{-}p\text{-cymene})(i\text{Pr-trisox})](PF_6)_2$ (**6**). The facial coordination of their three ligating atoms to a metal center may be impeded if the transition-metal center stereoelectronically strongly favors a non-deltahedral coordination sphere, which is generally the case for the heavier d^8-transition-metal atoms/ions. Reaction of *i*Pr-trisox with $[Rh(cod)_2]BF_4$ led to the formation of the 16-electron d^8-configured complex $[Rh(i\text{Pr-trisox})(cod)](BF_4)$ (**7**), which is oxidized by $CsBr_3$ to give the Rh^{III} complex $[RhBr_3(i\text{Pr-trisox})]$ (**8**) possessing a C_3-symmetric structure with a κ^3-*N*-trisox ligand. The crystalline salts $[M_2(\mu\text{-}Cl_3)(i\text{Pr-trisox})_2](PF_6)$ (M = Fe^{II}: **9**, Co^{II}: **10**, Ni^{II}: **11**), were prepared by addition of one molar equivalent of *i*Pr-trisox and an excess of KPF_6 to solutions of the anhydrous ($FeCl_2$) or hydrated metal halides ($CoCl_2\cdot 6H_2O$, $NiCl_2\cdot 6H_2O$). All dinuclear complexes display weak magnetic coupling. For the mononuclear species $[CuCl_2(i\text{Pr-trisox})]$ (**12**) the removal of a chloride anion and thus the generation of a dinuclear chloro-bridged structure failed due to Jahn–Teller destabilization of a potential octahedral coordination sphere.

Keywords: C_3 symmetry · chirality · coordination chemistry · transition-metal complexes · trisoxazolines · X-ray diffraction

[a] Prof. Dr. L. H. Gade, Dr. G. Marconi, Dr. B. D. Ward, Prof. Dr. H. Wadepohl
Anorganisch-Chemisches Institut, Universität Heidelberg
Im Neuenheimer Feld 270, 69120 Heidelberg (Germany)
Fax: (+49) 6221-545-609
E-mail: lutz.gade@uni-hd.de

[b] C. Dro, Dr. M. Poyatos, Dr. S. Bellemin-Laponnaz
Institut de Chimie, Université Louis Pasteur
4 rue Blaise Pascal, 67000 Strasbourg (France)
E-mail: bellemin@chimie.u-strasbg.fr

[c] Dr. L. Sorace, Dr. G. Poneti
Laboratory of Molecular Magnetism, UdR INSTM e Dipartimento di Chimica
Università degli Studi di Firenze
Via della Lastruccia 3, 50019 Sesto Fiorentino (Fi) (Italy)

Introduction

There has been considerable debate about the usefulness and potential advantages of C_3 symmetry in the design of chiral stereodirecting ligands for asymmetric catalytic reactions,[1–5] and in most cases this relates to facially coordinating tripodal ligands. Threefold rotational symmetry represents the only possibility adapted to this topology of ligation, in the same way that C_2 symmetry is related to simple chelation.[6]

Symmetry in a spectator ligand will only have an effect on the chemical reactions of its complexes if it is compatible with their respective molecular structure as a whole, that is, with the coordination geometry and the composition of the remaining "active" coordination sphere.[7] This given, a symmetrical stereodirecting ligand may lead to a reduced number of transition states and diastereomeric reaction intermediates in transformations occurring in the coordination sphere of its complexes. In favorable cases, this degeneration of alternative reaction pathways may lead to high stereoselectivity in catalytic reactions and greatly simplifies the analysis of such transformations.

For spectator ligands of podand topology and in complexes with coordination numbers greater than four, C_3-chiral tripods may play such a role.[8] A particularly versatile ligand system, which has the additional advantage of a modular assembly is the family of 1,1,1-trisoxazolinylethanes ("trisox") recently introduced by us.[9,10] Various derivatives of this ligand have been successfully employed in a wide variety of stereoselective transformations. These range from Cu^{I}-catalyzed cyclopropanations,[10] Zn^{II}-catalyzed transesterifications,[11] Sc^{III}- and lanthanide-catalyzed isotactic polymerization of α-olefins[12] to Cu^{II}-Lewis acid catalyzed reactions, such as Mannich reactions and asymmetric aminations with azodicarboxylates.[13] For the latter their bidentate coordination in the active species has been established, and the tripodal binding is only thought to stabilize the resting state.

Asymmetric catalysis with trisox complexes has thus involved both d-block metals and the lanthanides for which the metal centers may vary greatly in terms of their oxidation state and atomic or ionic radius. A question which arises is to which extent the new tripods may adapt to the "needs" of the metal and the structure of the remaining coordination sphere. This work provides the first systematic and comprehensive study into the coordination chemistry of this class of stereodirecting ligands. It also aims to establish several important points related to their chirality which is defined by the substitution patterns of the oxazoline rings. This includes the study of the feasibility of $\{M(trisox)_2\}$ species which might form in situ and which in applications in catalysis would represent *inactive* species. We also aim to establish and fully characterize structural alternatives which may arise in the complex assembly based on a trisox derivative and a metal salt.

The structural non-complementarity of two homochiral trisox ligands in $[M(trisox)_2]^{n+}$ complexes: A prerequisite for potential catalytic activity: A key feature of the trisox ligands is the orientation of the substituents at the chiral center in the 4-position of the oxazoline rings. This favors the formation of catalytically active complexes even for substitutionally labile transition metals which may readily undergo complex redistributions ("dismutations"). The steric demand of the substituent groups employed in this work, as well as their orientation relative to the molecular axis, renders the formation of "homoleptic" $[M(trisox)_2]^{n+}$ species unfavorable and thus stabilizes a coordination sphere which combines the stereodirecting tripod with up to three remaining ("active") coordination sites. This is the case, provided that the *enantiomerically pure* C_3-symmetric ligands or the stereochemically "mixed" (C_1-symmetric) derivatives (enantiomerically pure or racemic) are being employed.

The combinations of trisox ligands representing the different stereochemical possibilities are summarized in Figure 1, specifically emphasizing the consequences of the formation of potentially inactive $[M(trisox)_2]^{n+}$. Only for the racemate (*R,R,R* + *S,S,S*) of the C_3-chiral ligands is the formation of such a symmetric hexacoordinate complex expected to be favored (see bottom, first from the left). In such *meso*-$[M(trisox)_2]^{n+}$ complexes the orientation of the 4-oxazoline substituents is complementary and avoids significant repulsive interactions. In contrast, the combination of a homochiral pair of C_3-trisox ligands at a single metal center will generate three repulsive inter-ligand interactions (Figure 1, bottom: second from the left) and is thus expected to be disfavored. This is exactly the situation that would be encountered in the application of the enantiopure C_3-chiral trisoxazolines in catalytic transformations! Unfavorable interligand repulsion is also encountered in hetero- or homochiral combinations of the mixed-configuration C_1-trisox derivatives as is indicated in the third and fourth example at the bottom of Figure 1. This phenomenon has been recently discussed by Takacs et al. in relation to C_2-symmetric complexes.[14]

For divalent transition metals, for which an octahedral coordination sphere is strongly favored, the impossibility to form $[M(trisox)_2]^{n+}$ complexes with the enantiomerically pure tripods will lead to an alternative way of coordinative stabilization, and thus molecular structure, both in solution and in the solid state. Provided that the counterions may act as bridging ligands, as is the case for halides, the formation of dinuclear face-sharing bis(octahedral) complexes of the general type $[M_2(\mu\text{-}X)_3(trisox)_2]^{+}$ (X = halide) is strongly favored as will be shown below. However, if octahedral coordination at the metal center is stereoelectronically disfavored (as for d^8- and d^9-metal centers) other structural types are observed.

Results and Discussion

***C_3* versus *C_1* chirality: the modularity of the ligand assembly**: The possibility to combine oxazolines, in which the stereogenic centers adjacent to the N-donor atoms have differ-

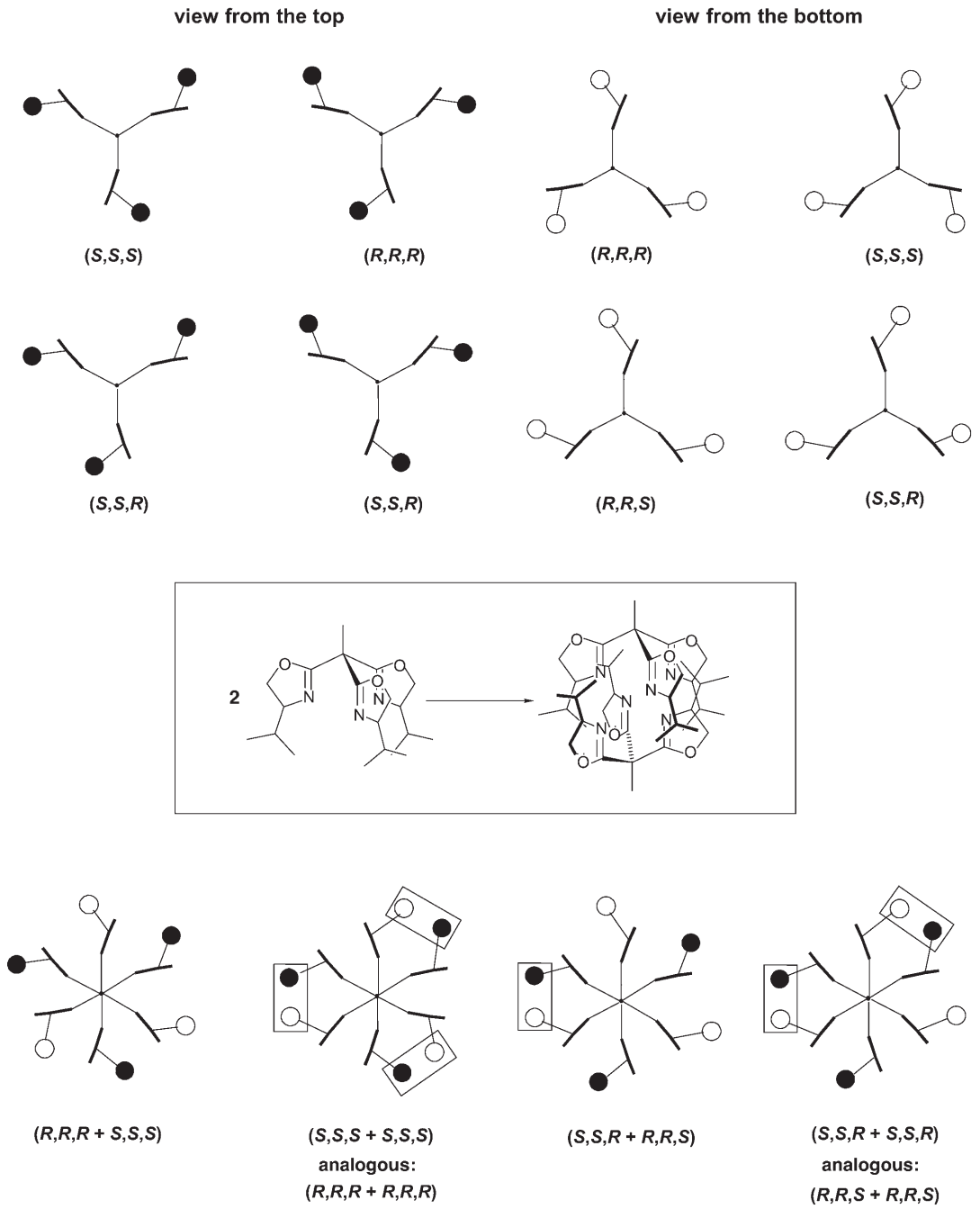

Figure 1. Shaping coordination spheres with chiral trisox derivatives: Modular assembly of C_3-chiral and mixed-stereochemically C_1-chiral tripods (top) and their possible combinations in $[M(trisox)_2]^{n+}$ complexes (middle), demonstrating the non-complementarity of two homochiral ligands in such species (bottom). Stability in this case is only expected for the heterochiral *meso* form (*R*,*R*,*R* + *S*,*S*,*S*; bottom left).

ent absolute configuration, within the trisox systems, whilst retaining their ability to coordinate as *tripodal* ligands, was demonstrated by reaction of the enantiomerically pure C_3-symmetric *i*Pr-trisox(*S*,*S*,*S*) and C_1-symmetric *i*Pr-trisox(*S*,*S*,*R*) with $[Mo(CO)_3(NCMe)_3]$ (Scheme 1). In both reactions the corresponding products were the tricarbonylmolybdenum complexes **1a** and **1b**, containing the trisox ligands in a facially coordinating mode which indicates the absence of significant repulsive interactions between the substituents (vide infra).

Whereas the ^1H and ^{13}C NMR spectra of **1a** are highly symmetrical as expected, and are consistent with the threefold molecular symmetry, the NMR spectra of **1b** indicate the reduced symmetry of the system which is already apparent in the data for the free C_1-symmetric mixed-configuration ligand *i*Pr-trisox(*S*,*S*,*R*). The IR spectra of both com-

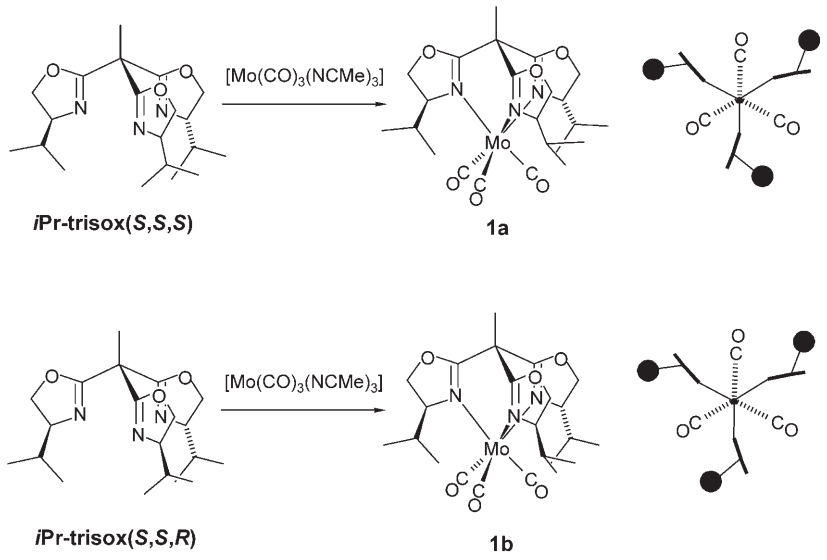

Scheme 1. Synthesis of the C_3-chiral [Mo{*i*Pr-trisox(*S,S,S*)}$(CO)_3$] (**1a**) and the C_1-chiral analogue [Mo{*i*Pr-trisox(*S,S,R*)}$(CO)_3$] (**1b**).

plexes display two stretching bands for the carbonyl ligands (**1a**: $\nu = 1889$, 1852, **1b**: 1902, 1890 cm^{-1}), representing the A + E stretching modes of facial $Mo(CO)_3$ units.

To compare the details of both molecular structures, single-crystal X-ray structure analyses of **1a** and **1b** were carried out. Views along the (threefold) molecular axis of both molecules (defined by the apical atom of the tripod and the central metal atom) are depicted in Figure 2. Both the ORTEP and the space-filling representations of the structures are consistent with the postulated independence of the oxazoline substituents and the absence of significant inter-oxazoline repulsion. This is corroborated by the N-Mo-N′ angles in the C_1-symmetric structure of **1b** which deviate only slightly from those in the threefold-symmetrical molecule of **1a**.

Both molecules have a distorted octahedral geometry with average N_{oxaz}–Mo and Mo–C bond lengths of 2.27 and 1.94 Å, respectively.[15] The N_{oxaz}-Mo-N'_{oxaz} angles ranging from 76.9 to 79.7°, deviate strongly from the expected right angles of an ideal octahedral arrangement, which is due to the steric constraints of the tripod combined with the large atomic radius of the zerovalent second-row transition metal. The latter is underscored by the interligand angles of the monodentate carbonyl ligands which are close to 90°.

A case of structural complementarity or non-complementarity: the stability and instability of homo- and heterochiral {(trisox)$_2$M} fragments: The synthesis of the racemic *i*Pr-trisox ligands was conducted starting from racemic valine (Scheme 2). The reaction of the resulting stereochemically non-uniform bisoxazoline with the corresponding racemic bromooxazoline led to a mixture of the racemic-C_3 symmetric trisoxazoline together with the racemic-C_1 symmetric trisoxazoline. The C_1/C_3 ratio was found to be 3:1, which is consistent with the predicted statistical ratio (considering that all diastereomers react at the same rate). Both diastereomers were readily separated and isolated from column chromatography on silica gel (EtOAc/MeOH). Notably, the *i*Pr-trisox(*rac*-C_3) ligand is obtained as a colorless crystalline solid at ambient temperature, in contrast to the enantiopure substance which is a liquid. An X-ray diffraction study of the racemate established for the first time the detailed structure of a free trisox derivative (for the crystal data, see Experimental Section).

The availability of *i*Pr-trisox(*rac*-C_3) enabled us to test the stereochemical considerations outlined in the introduction. Reaction of *i*Pr-trisox(*rac*-C_3) with one equivalent of $[Co(ClO_4)_2]\cdot 6H_2O$ in the ligating solvent acetonitrile led to the formation of *rac*-[Co(*i*Pr-trisox)$(NCCH_3)_3](ClO_4)_2$ (**2**), which was isolated as a pale pink crystalline solid (Scheme 3). Suitable crystals for X-ray diffraction were obtained from acetonitrile/diethyl ether. The structure of complex **2** is presented in Figure 3 along with the principal bond lengths and angles. As expected, the coordination geometry around the metal center is distorted octahedral with the trisox ligand binding facially and the three remaining positions being occupied by coordinating acetonitrile. The average $Co–N_{acetonitrile}$ and $Co–N_{oxaz}$ distances are both 2.1 Å, whilst the other structural features closely resemble those of the iron(II) analogue discussed in the following section.

The analogous reaction between *i*Pr-trisox(*rac*-C_3) and one equivalent of $[Co(ClO_4)_2]\cdot 6H_2O$ was carried out in dichloromethane as a non-coordinating solvent. Since we had observed previously that complexes of the composition $[M(trisox)(H_2O)_3]^{2+}$ of the first-row transition metals are substitutionally highly unstable, the system was thought to undergo redistribution to form a $[Co(trisox)_2]^{2+}$ species. Even after stirring for several hours, about 50% of the $[Co(ClO_4)_2]$ starting material remained suspended, whilst 0.5 molar equivalents of the Co^{2+} had rapidly dissolved upon formation of a trisox complex. A FAB mass spectrum of the isolated light pink cobalt coordination compound **3**, which possesses the spectral characteristics of a high-spin octahedral Co^{II} complex,[16] displayed a molecular ion at *m*/*z* 785.5, which corresponds to the {Co(*i*Pr-trisox)$_2$} cation. The characteristic isotopomer distribution of this molecular ion peak as well as the elemental analysis of the isolated complex are consistent with the formulation of **3** as [Co{*i*Pr-trisox(*R,R,R*)}{*i*Pr-trisox(*S,S,S*)}]$(ClO_4)_2$. The same product is obtained in quantitative yield (based on the Co^{2+}) if ligand and salt employed in the synthesis are allowed to react in a

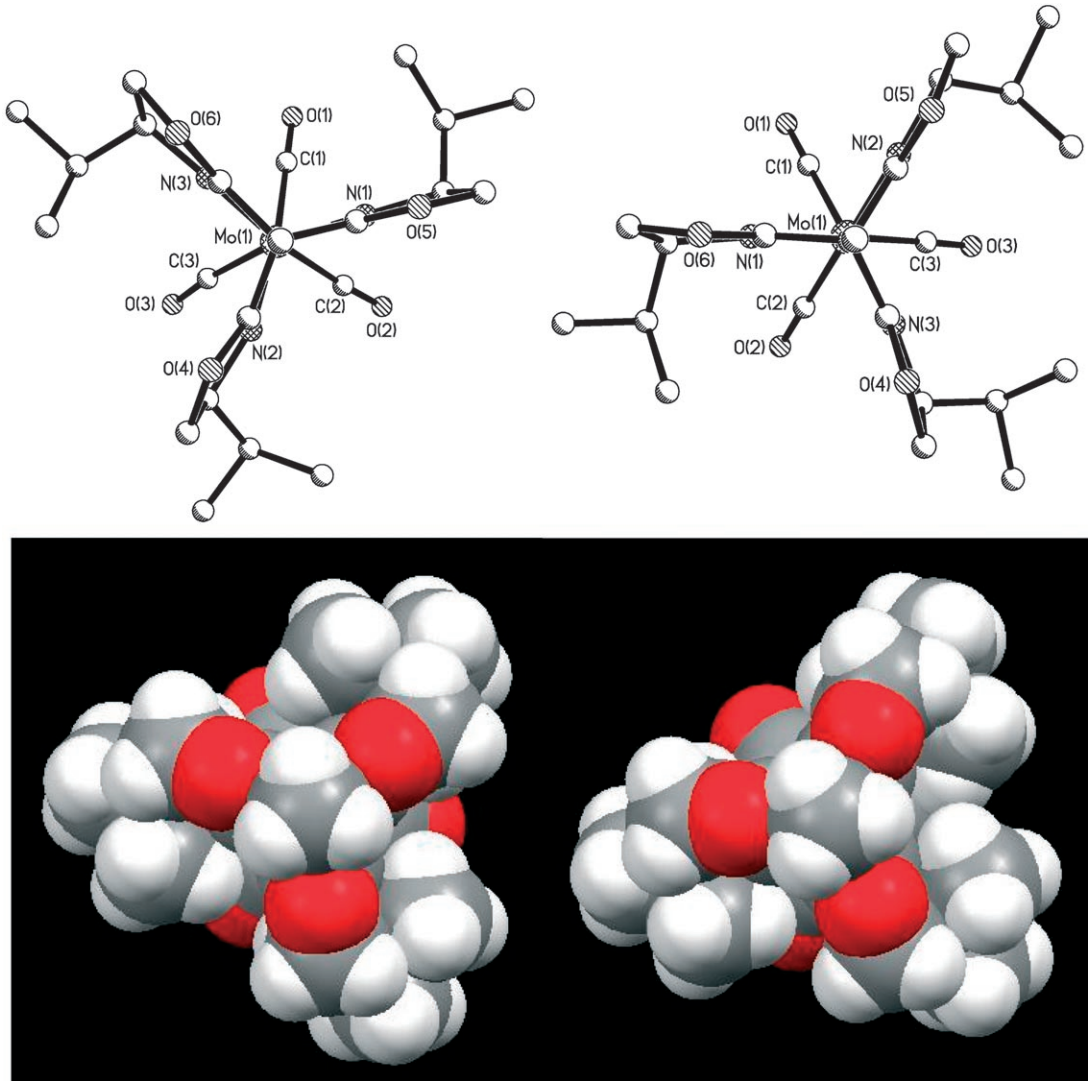

Figure 2. Molecular structures of the C_3-chiral complex [Mo{*i*Pr-trisox(*S,S,S*)}$(CO)_3$] (**1a**; left) and the C_1-chiral analogue [Mo{*i*Pr-trisox(*S,S,R*)}$(CO)_3$] (**1b**; right). Principal bond lengths [Å] and angles [°]: **1a**: Mo(1)–C(1) 1.949(3), Mo(1)–C(2) 1.944(3), Mo(1)–C(3) 1.939(3), Mo(1)–N(1) 2.245(2), Mo(1)–N(2) 2.268(2), Mo(1)–N(3) 2.288(3); C(3)-Mo(1)-C(2) 86.06(13), C(3)-Mo(1)-C(1) 89.55(12), C(2)-Mo(1)-C(1) 85.43(12), C(1)-Mo(1)-N(1) 99.99(11), C(2)-Mo(1)-N(2) 104.14(11), C(3)-Mo(1)-N(3) 103.43(11), N(1)-Mo(1)-N(2) 79.53(9), N(1)-Mo(1)-N(3) 79.25(9), N(2)-Mo(1)-N(3) 76.68(9). **1b**: Mo(1)–C(1) 1.945(8), Mo(1)–C(2) 1.949(8), Mo(1)–C(3) 1.924(9), Mo(1)–N(1) 2.281(6), Mo(1)–N(2) 2.286(6), Mo(1)–N(3) 2.265(5); C(1)-Mo(1)-C(2) 86.6(3), C(2)-Mo(1)-C(3) 83.9(3), C(1)-Mo(1)-C(3) 85.9(3), C(1)-Mo(1)-N(2) 97.6(3), C(2)-Mo(1)-N(1) 97.2(2), C(3)-Mo(1)-N(3) 97.2(3), N(1)-Mo(1)-N(2) 78.7(2), N(2)-Mo(1)-N(3) 79.7(2), N(1)-Mo(1)-N(3) 78.4(2).

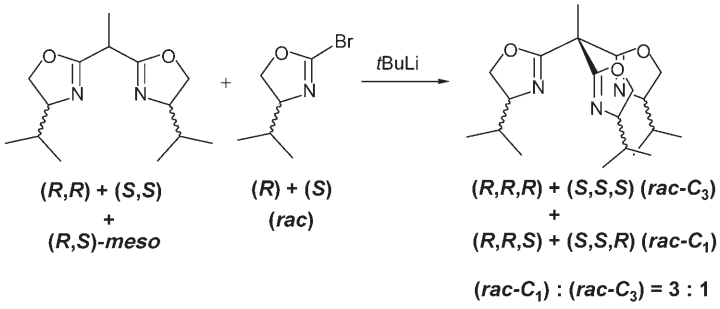

Scheme 2. Final step in the synthesis of the mixture of (*rac*-C_1)- and (*rac*-C_3)-trisox from racemic valinol.

2:1 molar ratio. Unfortunately, all attempts to grow crystals of **3**, which are suitable for X-ray diffraction, were unsuccessful.

In contrast, reaction of chiral *enantiopure* (*S,S,S*)-*i*Pr-trisox with half an equivalent of $[Co(ClO_4)_2]\cdot 6H_2O$ in dichloromethane led to the formation of a mixture of Co-(trisox) complexes, the FAB mass spectrum of which displayed a complex ion at *m*/*z* 520.9, corresponding to the $[(trisox)Co(ClO_4)]^+$ fragment. Notable is the total absence of a $[(trisox)_2Co]^{+/2+}$ ion which is consistent with its destabilization due to steric repulsion between the homochiral tripods, as delineated in the introduction.

To semi-quantitatively illustrate the effect of the chirality of the different trisox substituents on the stability of the

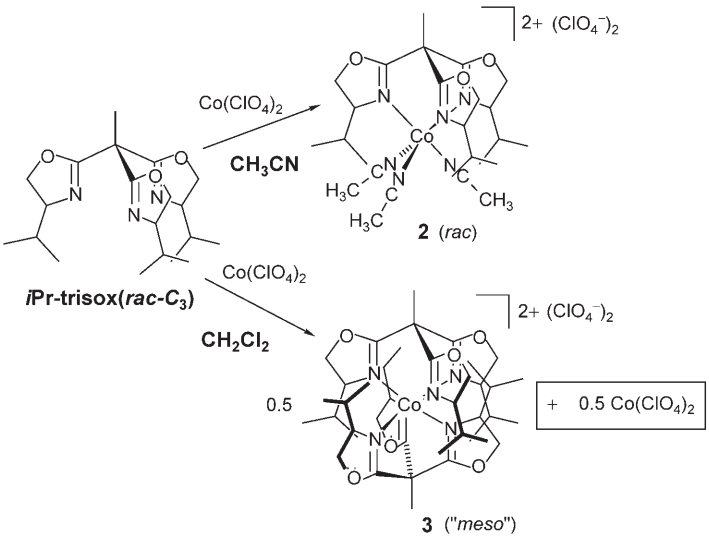

Scheme 3. Complexation of cobalt(II) with racemic *i*Pr-trisox in a coordinating solvent (MeCN) and a non-coordinating solvent (CH_2Cl_2). The former leads to *rac*-[Co(*i*Pr-trisox)$(NCMe)_3$]$(ClO_4)_2$ (**2**), whilst the latter gives the heterochiral ("*meso*") complex [Co{*i*Pr-trisox(*S,S,S*)}{*i*Pr-trisox(*R,R,R*)}]$(ClO_4)_2$ (**3**).

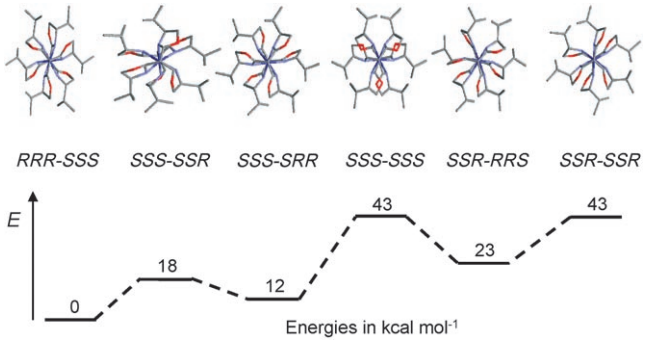

Figure 4. Molecular mechanics (UFF) study of the relative energies of various homo- and heterochiral combinations of C_3- and C_1-symmetrical *i*Pr-trisox ligands in [Co(*i*Pr-trisox)$_2$], illustrating the relative destabilization of all combinations except for the *meso* complex [Co{*i*Pr-trisox(*S,S,S*)}{(*i*Pr-trisox(*R,R,R*)}]$^{2+}$ on the left.

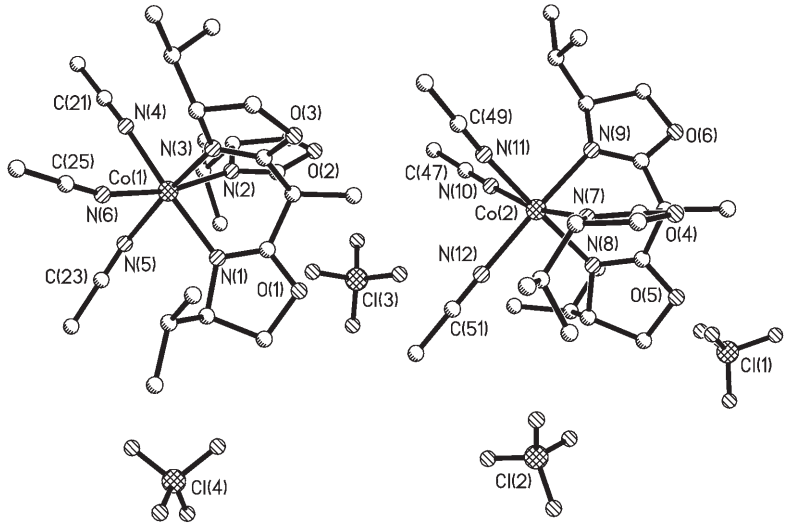

Figure 3. Molecular structures of the racemic pair of [Co(*i*Pr-trisox)$(NCMe)_3$]$(ClO_4)_2$ in compound **2**. Principal average bond lengths [Å] and angles [°] in both enantiomers: Co(1)–N(1) 2.120(2), Co(1)–N(2) 2.125(2), Co(1)–N(3) 2.144(2), Co(1)–N(4) 2.154(2), Co(1)–N(5) 2.139(2), Co(1)–N(6) 2.121(2); N(1)-Co(1)-N(2) 83.99(8), N(2)-Co(1)-N(3) 84.84(8), N(1)-Co(1)-N(3) 84.84(8), N(4)-Co(1)-N(5) 88.87(9), N(5)-Co(1)-N(6) 88.18(9), N(4)-Co(1)-N(6) 86.10(9); Co(2)–N(7) 2.097(2), Co(2)–N(8) 2.187(2), Co(2)–N(9) 2.134(2), Co(2)–N(10) 2.140(2), Co(2)–N(11) 2.168(3), Co(2)–N(12) 2.104(3); N(7)-Co(2)-N(9) 86.00(9), N(7)-Co(2)-N(8) 83.77(9), N(8)-Co(2)-N(9) 83.99(8), N(10)-Co(2)-N(12) 87.37(9), N(11)-Co(2)-N(12) 91.18(9), N(10)-Co(2)-N(11) 85.80(9).

"homoleptic" complexes, the various trisox combinations in the complexes [Co(*i*Pr-trisox)$_2$]$^{2+}$ in Figure 1 were simulated using molecular mechanics (UFF) calculations. The energies of the mononuclear complexes [Co(*i*Pr-trisox)$_2$]$^{2+}$ (relative to the {*S,S,S-R,R,R*} complex) are displayed in Figure 4. Although these energies cannot be compared with great precision in absolute terms, they nevertheless provide a useful guide as to the relative steric repulsion exerted by the trisox isopropyl substituents.

Confirming the qualitative considerations outlined above, the stability of the complexes decreases in the order {*S,S,S-R,R,R*}, {*S,S,R-R,R,S*}, {*S,S,R-S,S,R*}, {*S,S,S-S,S,S*}, consistent with an increasing number of unfavorable interactions (0, 1, 2, and 3 respectively, Figure 1) between the oxazoline substituents. The most remarkable feature is that the energy of the {*S,S,S-S,S,S*} isomer (three unfavorable repulsive interactions) is essentially identical to that of the {*S,S,R-S,S,R*} isomer (only two). This is readily understood, since an analysis of the calculated minimum-energy structure indicates that the oxazoline rings are significantly more "twisted" in the {*S,S,S-S,S,S*} complex (to alleviate steric strain) than in the *SSR-SSR* complex. A greater degree of twisting is presumably possible in the complexes with C_3-symmetric ligands, since the coordination environment of the tripodal ligand allows only the "concerted" rotation of all oxazolines. In [Co(trisox)$_2$]$^{2+}$ complexes containing stereochemically mixted C_1-symmetric ligands twisting of the oxazolines will reduce steric interactions in one part of the molecule whilst increasing it in another. These open shell systems proved to be too complex for treatment with DFT or ONIOM methods, although the corresponding diamagnetic zinc complex [Zn{*i*Pr-trisox(*S,S,S*)}{*i*Pr-trisox(*R,R,R*)}]$^{2+}$ was calculated as a model using ONIOM methodology and confirmed the val-

idity of the structural features; the zinc analogues of the other isomeric forms failed to give converged structures.

Synthesis and structural characterization of mononuclear {(trisox)M} complexes: To demonstrate the scope of the trisox ligand in terms of facial coordination to both early and late transition metals, the mononuclear complexes $[ScCl_3(i\text{Pr-trisox})]$ (**4**), $[Fe(t\text{Bu-trisox})(NCMe)_3](BF_4)_2$ (**5**), and $[Ru(\eta^6\text{-}p\text{-cymene})(i\text{Pr-trisox})](PF_6)_2$ (**6**) were synthesized as shown in Scheme 4.

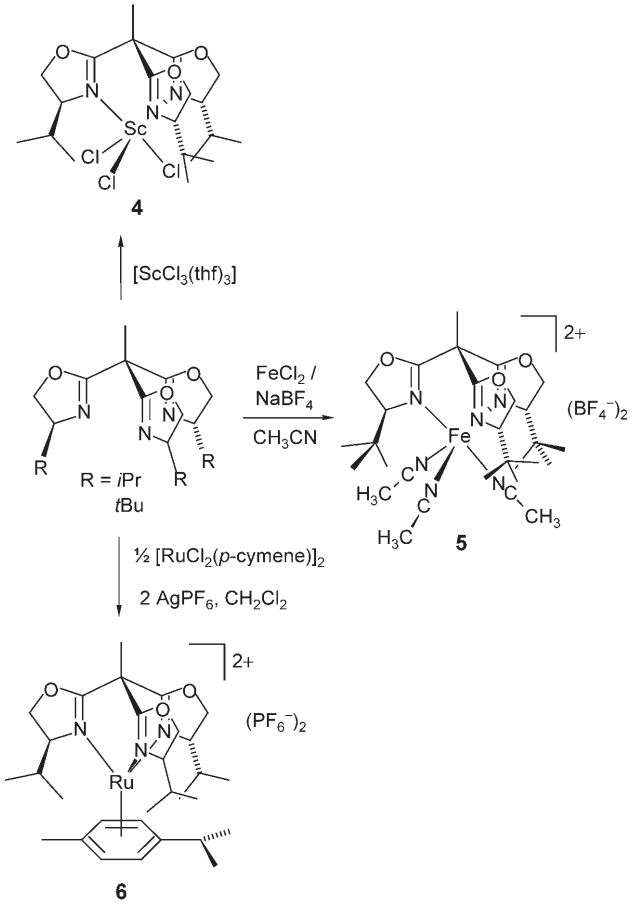

Scheme 4. Synthesis of the mononuclear complexes **4**–**6**.

Whereas the scandium complex **4** was obtained by reaction of *i*Pr-trisox with $[ScCl_3(thf)_3]$, the paramagnetic (high-spin d^6) iron dication **5** was isolated from a solution of *t*Bu-trisox, $FeCl_2$, and $NaBF_4$ in acetonitrile after removal of the NaCl precipitate by filtration. The dicationic complex $[Ru(\eta^6\text{-}p\text{-cymene})(i\text{Pr-trisox})](PF_6)_2$ (**6**) was synthesized by reaction of $[Ru(p\text{-cymene})Cl_2]_2$ with two equivalents of *i*Pr-trisox followed by the addition of $AgPF_6$. All complexes, which were isolated as highly crystalline solids, were characterized by ^1H and ^{13}C NMR spectroscopy as well as mass spectrometry, and gave satisfactory elemental analysis.

To compare their molecular structures, X-ray diffraction studies of all three compounds were carried out. The molecular structure of **4** is depicted in Figure 5, along with select-

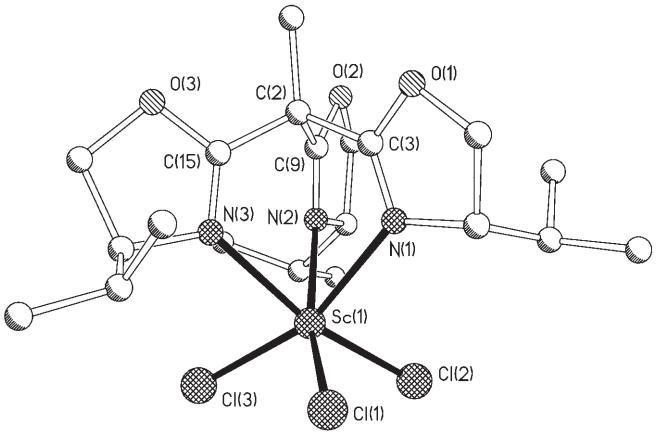

Figure 5. Molecular structure of $[ScCl_3(i\text{Pr-trisox})]$ (**4**). Principal bond lengths [Å] and angles [°]: Sc(1)–N(1) 2.346(3), Sc(1)–N(2) 2.324(3), Sc(1)–N(3) 2.295(2), Sc(1)–Cl(1) 2.403(1), Sc(1)–Cl(2) 2.413(1), Sc(1)–Cl(3) 2.398(1); Cl(1)-Sc(1)-Cl(2) 98.40(3), Cl(1)-Sc(1)-Cl(3) 102.90(4), Cl(2)-Sc(1)-Cl(3) 99.17(4), N(1)-Sc(1)-N(2) 75.62(9), N(1)-Sc(1)-N(3) 77.88(9), N(2)-Sc(1)-N(3) 78.19(9).

ed bond lengths and angles. The central scandium atom exhibits a highly distorted octahedral coordination geometry, as evidenced by the angles subtended at the scandium center, which are significantly distorted away from the ideal 90°. The very small N-Sc-N angles (N(1)-Sc-N(2) 75.6(1), N(2)-Sc(1)-N(3) 77.9(1), N(1)-Sc(1)-N(3) 78.2(1)°) contrast with the other X-ray analyses reported herein, which are typically in the range of 83–86°. The Sc–N and Sc–Cl bond lengths are unremarkable in comparison to previously reported examples,[17] which is presumably attributed to the small size of the scandium. Mutual steric repulsion of the chloride ligands leads to markedly increased inter-halide angles (98°–103°), which in turn "pushes" the N_3Sc unit together.

Suitable crystals for X-ray diffraction of the iron complex $[Fe(t\text{Bu-trisox})(NCMe)_3](BF_4)_2$ (**5**) were obtained from acetonitrile/diethyl ether layering. The molecular structure of the dication is shown in Figure 6. As for the other mononuclear complexes, the coordination geometry around the metal is distorted octahedral with the trisox ligand binding facially and the three remaining positions being occupied by coordinating acetonitrile. From the Fe–N_{oxaz} bond lengths, it can be deduced that compound **5** has a high-spin iron(II) center (bond lengths averaging 2.2 Å),[18] which is consistent with the observed paramagnetism of the complex. The average Fe–$N_{acetonitrile}$ distance is 2.1 Å. An acute N_{oxaz}-Fe-N_{oxaz} average angle of 84.5° is observed due to the chelating effect of the ligand, while the average N-Fe-N′ angle of 89.2° between the acetonitrile ligands is close to the expected value for an octahedral complex. The complex was found to be very sensitive to air both in the solid state and in solution.

Crystals of compound **6** contained two crystallographically independent molecules in the asymmetric unit with no significant differences between them. The molecular structure of one of these is displayed in Figure 7 along with the princi-

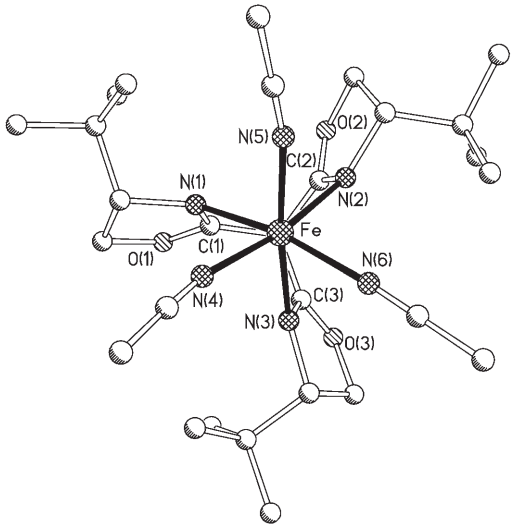

Figure 6. Molecular structure of the $[Fe(i\text{Pr-trisox})(NCMe)_3]^{2+}$ dication in **5**. Principal bond lengths [Å] and angles [°]: Fe–N(1) 2.258(2), Fe–N(2) 2.205(2), Fe–N(3) 2.215(2), Fe–N(4) 2.131(2), Fe–N(5) 2.171(2), Fe–N(6) 2.163(2); N(4)-Fe-N(5) 86.01(9), N(4)-Fe-N(6) 90.26(9), N(5)-Fe-N(6) 91.34(8), N(1)-Fe-N(3) 82.12(6), N(1)-Fe-N(2) 84.62(6), N(2)-Fe-N(3) 86.88(7), N(1)-Fe-N(4) 90.54(7).

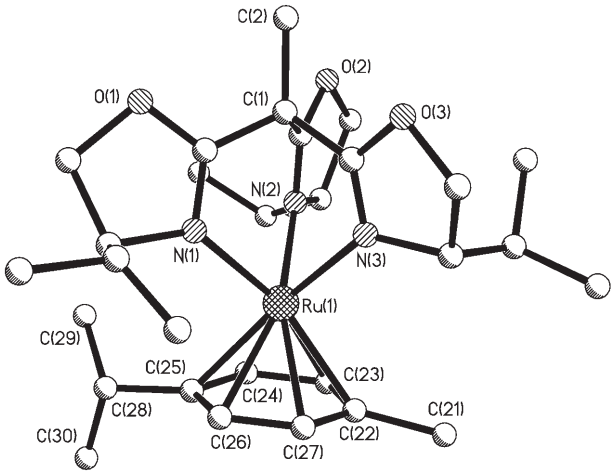

Figure 7. Molecular structure of $[Ru(i\text{Pr-trisox})(\eta^6\text{-}p\text{-cymene})]^{2+}$ (**6**). Principal bond lengths [Å] and angles [°]: Ru(1)–N(1) 2.14(1), Ru(1)–N(2) 2.144(10), Ru(1)–N(3) 2.150(9), Ru(1)–C(22) 2.225(13), Ru(1)–C(23) 2.199(12), Ru(1)–C(24) 2.191(9), Ru(1)–C(25) 2.254(10), Ru(1)–C(26) 2.198(10), Ru(1)–C(27) 2.198(11); N(1)-Ru(1)-N(2) 84.8(8), N(1)-Ru(1)-N(3) 80.7(3), N(2)-Ru(1)-N(3) 79.6(4), C(25)-Ru(1)-C(23),67.3(4), N(1)-Ru(1)-C(24) 121.8(4).

pal bond lengths and angles. In the molecule, which is displayed in Figure 7, the average N-Ru-N′ angle of 81.7° for the coordinated *i*Pr-trisox ligand is slightly more acute than typically found for late d-block metals. This is thought to be a consequence of inter-ligand repulsion between the tripod and the η^6-coordinated cymene ligand, which is also reflected in the slightly non-symmetrical coordination of the π-arene ligand. Nevertheless, the $Ru{-}C_{arene}$ bond lengths of between 2.19 and 2.25 Å are well within the range normally observed for this complex fragment.[19]

In summary, this crystallographic study demonstrates the propensity of the trisox ligand system to bind facially to d-block metals of variable atomic/ionic radii provided that the central metal stereoelectronically favors this coordination mode (vide infra). The tripodal coordination mode adjusts itself to the metal center allowing a significant variation of the metric parameters (M–N distances and N-M-N′ angles).

The role of stereoelectronics at the metal center: going from di- to tridentate coordination of the trisox ligand upon oxidative addition to rhodium(I): Tripodal ligands are generally employed to enforce the facial coordination of their three ligating atoms to a metal center.[7,20] The formation of this structural motif may be impeded if the transition-metal center stereoelectronically strongly favors a non-deltahedral coordination sphere. This is generally the case for the heavier d^8-transition metal atoms/ions and their preference for square-planar coordination geometries. However, there are cases in which this is "overruled" by either the strong ligating tendency of the donor functions or inter-ligand angles of significantly below 90° which are enforced by a chelating coordination. An example for the former is the well established Rh^I complex chemistry with the triphos ligand and many of its derivatives and variants,[21] whereas nitrogen donor based tripods tend to favor a simple bidentate chelating coordination to rhodium(I), leaving one ligand "arm" non-coordinated. This has been observed both for neutral trispyridylmethane–[22] and trispyrazolylmethane–rhodium(I) complexes[23] as well as for their monoanionic trispyrazolylborate analogues.[24] To assess the coordinating behavior of the trisox ligands towards metal centers that favor or disfavor facial coordination, depending on their oxidation state (and thus d-electron count), we investigated the coordination chemistry of *i*Pr-trisox with rhodium(I) and (III).

Reaction of *i*Pr-trisox with $[Rh(cod)_2]BF_4$ in dry dichloromethane led to the formation of the $[Rh(i\text{Pr-trisox})(cod)](BF_4)$ (**7**) which was isolated as a yellow crystalline solid (Scheme 5). Suitable crystals for X-ray diffraction were obtained by slow diffusion from a solution in THF which was layered with diethyl ether. The structure of complex **7** is presented in Figure 8 along with the principal bond lengths and angles.

The 16-electron d^8-configured rhodium(I) complex adopts a (distorted) square-planar coordination geometry (as opposed to a potential five-coordinate trigonal-bipyramidal or square-pyramidal structure), which is reminiscent of the bisoxazoline derivative reported recently by Pregosin et al.[25] Two of the oxazoline groups are coordinated to the metal center (Rh–N bonds lengths: 2.11 and 2.09 Å), whereas the third oxazoline ring is twisted orthogonally with the N-donor unit pointing away from the metal center. The nitrogen-metal-nitrogen angle was found to be 85.2°. The 1,5-cod ligand is slightly twisted probably due to steric repulsion by the isopropyl groups of the oxazoline ligand. The six-membered ring formed by the metal and the chelating ligand adopts a boat conformation.

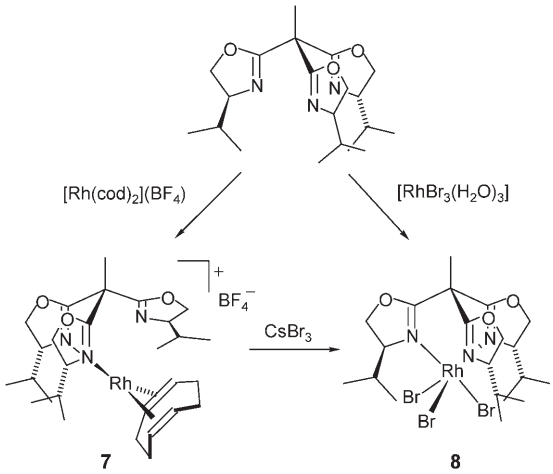

Scheme 5. Synthesis [Rh(*i*Pr-trisox)(cod)](BF_4) (**7**) and its reaction by way of oxidative addition with $CsBr_3$ giving the octahedral complex [$RhBr_3$(*i*Pr-trisox)] (**8**).

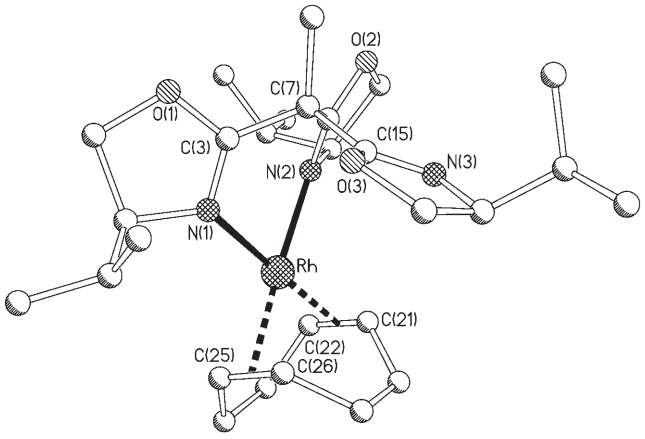

Figure 8. Molecular structure of the [Rh(*i*Pr-trisox)(cod)]$^+$ ion in **7**. Principal bond lengths [Å] and angles [°]: Rh–N(1) 2.11(1), Rh–N(2) 2.09(1), Rh–N(3) 3.70(1), Rh–C(21) 2.13(2), Rh–C(22) 2.14(2), Rh–C(25) 2.18(2), Rh–C(26) 2.09(2); N(1)-Rh-N(2) 85.1(6), C(21)-Rh-C(26) 80.9(7), C(22)-Rh-C(25) 81.6(8).

We note that the overall arrangement of the coordinated bisoxazoline unit in **7** is such that the uncoordinated oxazoline ring points towards the Rh atom. Thus, the unbound oxazoline appears to be ready to exchange with a coordinated heterocycle suggesting a potentially fluxional structure with a very low energy barrier for chemical exchange. The ^{1}H NMR spectrum recorded at 298 K was found to be highly symmetric and consistent with an effective local threefold symmetry of the trisox ligand. This equivalence of all three oxazolines on the NMR time scale at room temperature indicates the dynamic process suggested above. Even at a temperature of 193 K no broadening of the resonances is observed, which is consistent with a rapid dynamic exchange and an activation barrier $\Delta G^{\neq}$ of below 10 kcal mol^{-1}.

A possible way to get all the three oxazolines of *i*Pr-trisox coordinated to rhodium is the oxidation of the rhodium(I) complex to rhodium(III). A clean oxidation of **7** was achieved by stoichiometric reaction with $CsBr_3$ which acts both as an oxidant and ligand-transfer reagent (Scheme 5). The resulting Rh^{III} complex [$RhBr_3$(*i*Pr-trisox)] (**8**), which could be independently obtained by reaction *i*Pr-trisox with [$RhBr_3(H_2O)_3$], has very similar spectroscopic data to its chloro analogue[10] and was fully characterized by X-ray diffraction. Its molecular structure is represented in Figure 9 along with the principal bond lengths and angles.

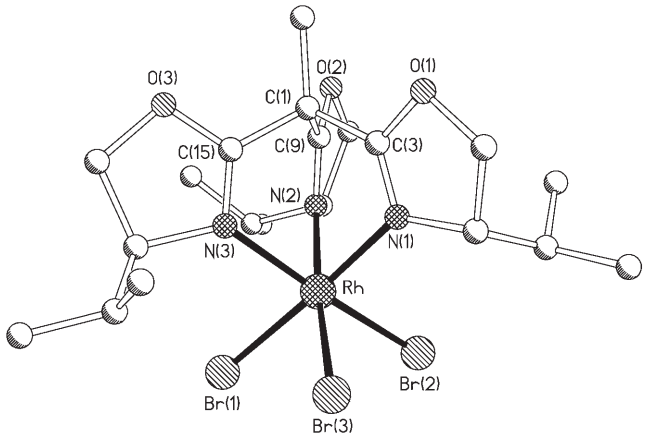

Figure 9. Molecular structure of [$RhBr_3$(*i*Pr-trisox)] (**8**). Principal bond lengths [Å] and angles [°]: Rh–Br(1) 2.4673(5), Rh–Br(2) 2.4715(5), Rh–Br(3) 2.4636(6), Rh–N(1) 2.073(4), Rh–N(2) 2.091(4), Rh–N(3) 2.084(3); Br(1)-Rh-Br(2) 89.59(2), Br(1)-Rh-Br(3) 90.49(2), Br(2)-Rh-Br(3) 92.35(2), N(1)-Rh-N(2) 85.9(1), N(1)-Rh-N(3) 86.3(1), N(2)-Rh-N(3) 84.1(1).

Compound **8** possesses a C_3-symmetric structure that is similar to the molecular structures discussed in the previous section. All metric parameters, in particular the Rh–Br bond lengths of 2.46 Å, lie within the expected range (Rh–Br 2.433–2.723, mean 2.528 Å for 110 examples).[26]

The transformation described in this section has shown that the coordination mode of the trisox ligand will adapt to the stereoelectronic requirements of the metal center and may change in the process of an elementary transformation such as the oxidative addition of bromine. This may be viewed as a model reaction for such reaction steps in a catalytic cycle. If the stereoselectivity determining step involves an octahedral species, the facial coordination of the trisox ligand and consequent threefold symmetry of the trisox–metal fragment will simplify the "stereoselection", whilst the symmetry of the ligand will act "dynamically" in species in which it is bidentate. The latter has been observed in Cu^{II}- and Pd$^{0/II}$-catalyzed transformations.[9,13,27,28]

The synthesis, crystal structures and magnetic properties of the dinuclear complexes [{(*i*Pr-trisox)M}$_2$(μ-Cl)$_3$]PF_6: As pointed out above, divalent transition-metal halides have the tendency to form halide-bridged face-sharing bisoctahedral complexes which avoids the unfavorable formation of [M(trisox)$_2$]$^{n+}$ species. A UFF molecular mechanics study

carried out for the chloro-bridged dimers $[Co_2(\mu\text{-}Cl)_3(i\text{Pr-trisox})_2]^+$ revealed much lower overall energy differences for the different isomeric forms than found for the mononuclear $[Co(i\text{Pr-trisox})_2]^{2+}$ complexes, as expected considering that the trisox ligands are significantly further removed from each other.[29]

The crystalline salts $[M_2(\mu\text{-}Cl_3)(i\text{Pr-trisox})_2](PF_6)$ (M = Fe^{II}, Co^{II}, Ni^{II}), were prepared by addition of one molar equivalent of *i*Pr-trisox and an excess of KPF_6 to solutions of the anhydrous ($FeCl_2$) or hydrated metal halides ($CoCl_2\cdot 6H_2O$, $NiCl_2\cdot 6H_2O$) (Scheme 6). After removal of insoluble residues by filtration, the salts were isolated upon diffusion of diethyl ether or hexane into dichloromethane solution of the complexes giving the reaction products in yields between 66 and 79%.

The dinuclear cation $[Ni_2(\mu\text{-}Cl_3)(i\text{Pr-trisox})_2]^+$ was also obtained by reaction of *i*Pr-trisox with one equivalent of $[NiCl_2(PPh_3)_2]$ in refluxing ethanol. Green crystals of the chloride salt $[Ni_2(\mu\text{-}Cl_3)(i\text{Pr-trisox})_2]Cl\cdot 3\,EtOH$ (**11a**) were isolated upon slow evaporation of the solvent after the reaction. Not unexpectedly, all attempts to force the d^9-metal copper(II) into a similar coordination environment failed. Whereas $CuCl_2$ is readily coordinated by *i*Pr-trisox, yielding the mononuclear species $[CuCl_2(i\text{Pr-trisox})]$ (**12**), the removal of a chloride anion by means of $NaBF_4$ or KPF_6 in hot alcohol (MeOH or EtOH) and thus the generation of a dinuclear chloro-bridged structure failed.

The iron complex **9** is colorless and displays no absorption in the 350–1000 nm range with $\varepsilon > 5\,L\,mol^{-1}\,cm^{-1}$, whereas the absorption bands of the nickel complex **11** at 407.7 nm ($\varepsilon = 26$) and 675.6 nm ($\varepsilon = 11$) are typical of d^8 octahedral nickel.

The crystal structures of the isostructural series of complexes **9**, **10**, and **11**, as well as **11a** and **12** have been determined by single-crystal X-ray diffraction. The three PF_6 salts of the dinuclear cations, **9**–**11**, crystallize in orthorhombic space groups ($P2_12_12_1$ for **9** and **10** and $C222_1$ for **11**), which differ in terms of the solvents incorporated into the unit cell. Each structure exhibits well-separated $[M_2(\mu\text{-}Cl_3)(i\text{Pr-trisox})_2]^+$ monocations and PF_6^- ions. As a representative example for the dinuclear complexes, the molecular structure of the Co_2 cation in compound **10** is depicted in Figure 10.

The dinuclear cations consist of two enantiomerically pure {(*i*Pr-trisox)M} units in which the tripodal ligand is bound facially to the metal in a tridentate fashion and which are connected by three bridging chloride ligands. The coordination environment about each metal center can thus be described as distorted octahedral. This is apparent in the view of the complex cation of **10** orthogonal to the metal–metal vector which is shown in Figure 10a. A closer inspection of the $[N_3M(\mu\text{-}Cl_3)MN_3]$ cores revealed an elongation of the N_3MCl_3 octahedron along the molecular threefold axis, which is slightly different for the two metal centers, reducing the overall molecular symmetry from D_3 to C_3 symmetry. The threefold molecular symmetry is readily appreciated in the view along the molecular axis of **10** depicted in Figure 10b, and a comparison of the key metric parameters of the dinuclear complex cations is provided in Table 1.

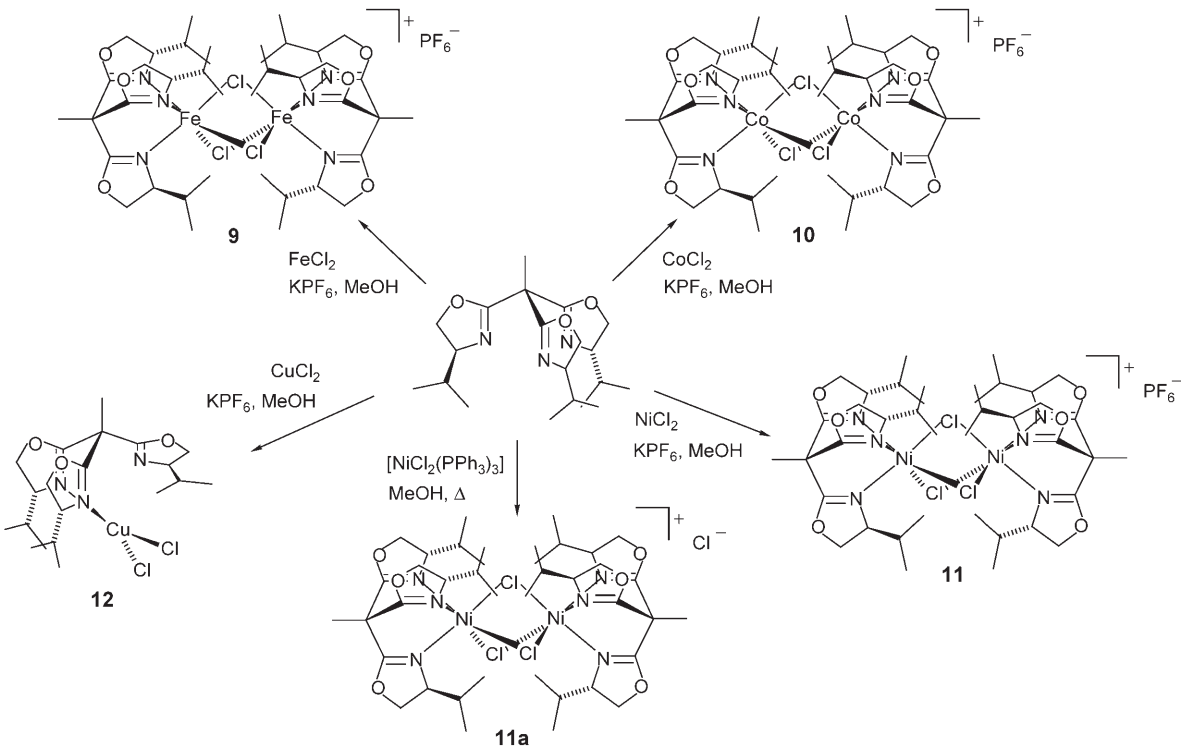

Scheme 6. Synthesis of the dinuclear complexes $[M_2(\mu\text{-}Cl)_3(i\text{Pr-trisox})_2]^+(A)^-$ (M = Fe, A = PF_6: **9**, Co, PF_6: **10**, Ni, PF_6: **11**, Ni, Cl: **11a**) and of $[CuCl_2(i\text{Pr-trisox})]$.

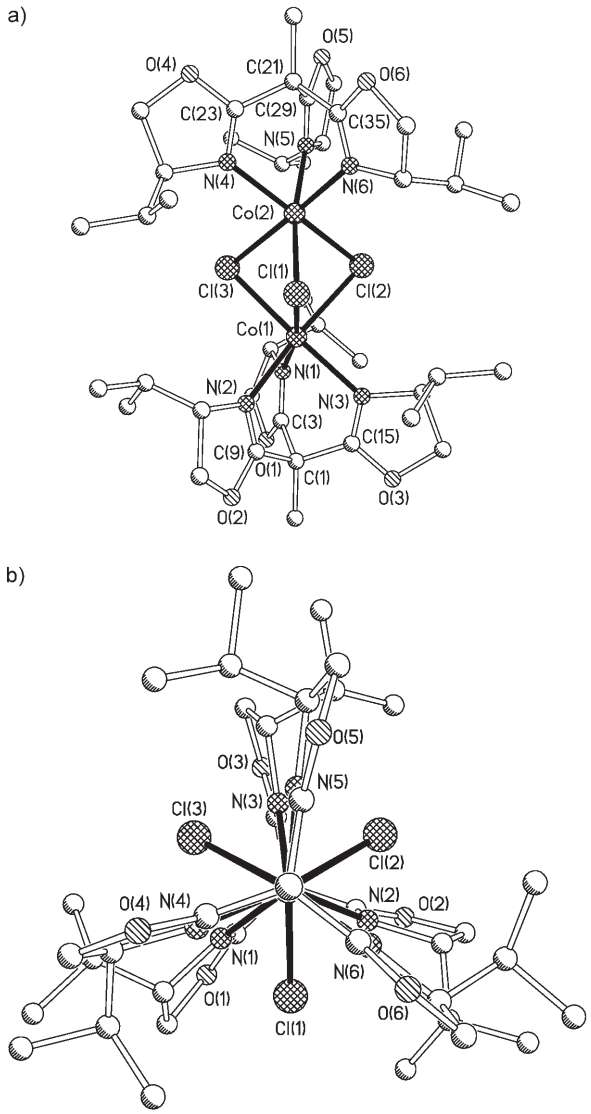

Figure 10. a) Molecular structure of $[Co_2(\mu\text{-}Cl)_3(i\text{Pr-trisox})_2]^+$ in **10**. The structures of the cations in the iron analogue **9** and the Ni complexes **11** and **11a** are very similar. A comparative listing of the principal metric parameters is provided in Table 1. b) View along the molecular axis illustrating the overall threefold symmetry of the molecule.

As for the individual structures, the diiron complex **9** was found to be slightly distorted along the molecular axis, the mean value of the Fe(1)–Cl distances being 2.482(6) Å, whereas the average for the Fe(2)–Cl distances is 2.502(2) Å. This non-equivalence is less pronounced for the Fe–N distances (Fe(1)–N_{av} 2.185, Fe(2)–N_{av} 2.176 Å). Similar distortions have been observed also by Sobota et al.[30] in the dinuclear complex $[(thf)_6Fe_2(\mu\text{-}Cl_3)]^+$ and by Wieghardt and co-workers[31] for $[(Me_3tacn)_2Fe_2(\mu\text{-}Cl_3)]^+$ (Me_3tacn = 1,4,7-trimethyl-1,4,7-triazacyclononane). The Fe(1)–Fe(2) separation of 3.028 Å is shorter than the intermetallic distance of 3.086 Å found for $[(thf)_6Fe_2(\mu\text{-}Cl_3)]^+$, while being similar to that for $[(Me_3tacn)_2Fe_2(\mu\text{-}Cl_3)]^+$ (3.026 Å).

The X-ray analyses of the dicobalt complex **10** and the dinickel complexes **11** and **11a** exhibit an almost identical structure for the cationic moieties. In addition, the crystals of **10** were found to be isotypic to those of **9**, although there was no pronounced distortion along the molecular axis as found for the iron complex. The metric parameters of **10** and **11** are all within expected ranges and, in particular, are similar to those observed for the $[(Me_3tacn)_2Co_2(\mu\text{-}Cl_3)]^+$ ion.[31]

Table 1. Comparison of the principal bond lengths and angles of the dinuclear complexes **9**–**11a**.

	9	**10**	**11**	**11a**[a]
M(1)–N(1)	2.168(6)	2.122(5)	2.072(3)	2.094(3)[b]
M(1)–N(2)	2.202(6)	2.136(5)	2.093(3)	–
M(1)–N(3)	2.185(8)	2.153(5)	2.082(3)	–
M(2)–N(4)	2.178(6)	2.133(5)	2.089(3)	2.104(3)[c]
M(2)–N(5)	2.176(6)	2.164(5)	2.101(3)	–
M(2)–N(6)	2.173(6)	2.111(5)	2.092(3)	–
M(1)–Cl(1)	2.488(2)	2.447(2)	2.4272(10)	2.4247(11)
M(1)–Cl(2)	2.467(2)	2.457(2)	2.4168(10)	–
M(1)–Cl(3)	2.493(2)	2.480(2)	2.4283(10)	–
M(2)–Cl(1)	2.507(2)	2.477(2)	2.4496(10)	2.4335(10)
M(2)–Cl(2)	2.502(2)	2.437(2)	2.4132(10)	–
M(2)–Cl(3)	2.497(2)	2.457(2)	2.4301(10)	–
N(1)-M(1)-N(2)	84.9(2)	84.2(2)	84.77(13)	85.14(11)[d]
N(1)-M(1)-N(3)	83.3(3)	82.5(2)	85.24(12)	–
N(2)-M(1)-N(3)	82.7(3)	84.3(2)	85.24(13)	–
N(4)-M(2)-N(5)	83.4(2)	82.7(2)	84.79(13)	84.66(11)[e]
N(4)-M(2)-N(6)	82.8(2)	86.5(2)	86.29(13)	–
N(5)-M(2)-N(6)	81.3(2)	82.8(2)	86.19(13)	–
M(1)-Cl(1)-M(2)	74.64(7)	76.70(5)	76.18(3)	77.06(4)
M(1)-Cl(2)-M(2)	75.10(7)	77.24(5)	77.05(3)	–
M(1)-Cl(3)-M(2)	74.73(7)	76.45(5)	76.52(3)	–
Cl(1)-M(1)-Cl(2)	87.46(8)	85.67(5)	85.45(3)	85.48(4)[f]
Cl(1)-M(1)-Cl(3)	87.24(7)	85.92(5)	85.74(4)	–
Cl(2)-M(1)-Cl(3)	87.36(7)	84.59(5)	86.18(4)	–
Cl(1)-M(2)-Cl(2)	86.26(7)	85.46(6)	85.04(3)	85.10(4)[g]
Cl(1)-M(2)-Cl(3)	86.73(6)	85.76(5)	85.21(4)	–
Cl(2)-M(2)-Cl(3)	86.49(8)	85.53(5)	86.22(3)	–

[a] Molecule lies on a crystallographic C_3 axis: values not given are identical to the stated values. [b] Ni(2)–N(1). [c] Ni(1)–N(2). [d] N(2)-Ni(1)-N(2A). [e] N(1)-Ni(2)-N(1A). [f] Cl(1)-Ni(1)-Cl(1A). [g] Cl(1)-Ni(2)-Cl(1A).

Triply choro-bridged dinuclear complexes of the first-row transition metals with facially fused bisoctahedral coordination geometries have been the object of detailed studies into their magnetic behavior. This especially applies to the complexes of the general type $[M_2(\mu\text{-}Cl_3)(thf)_6]^+$ and $[M_2(\mu\text{-}Cl_3)(Me_3tacn)_2]^+$ referred to above.[30,31] To relate the dinuclear compounds **9**–**11** to these previously reported systems, we carried out a comparative study of their magnetic properties.

All three complexes display Curie magnetism in solution and in the crystalline state at temperatures above 100 K. Rapid relaxation of the unpaired electrons in all three dinuclear complexes permit the recording of paramagnetic ^{1}H NMR spectra of **9**–**11**.[32] However, only the spectra of the cobalt complex displayed resonances that were sufficiently sharp to permit a partial assignment and a variable-temperature study of the paramagnetic shift. The ^{1}H NMR spectrum of **10** recorded at 295 K is displayed in Figure 11a, whilst the temperature dependence of the paramagnetic

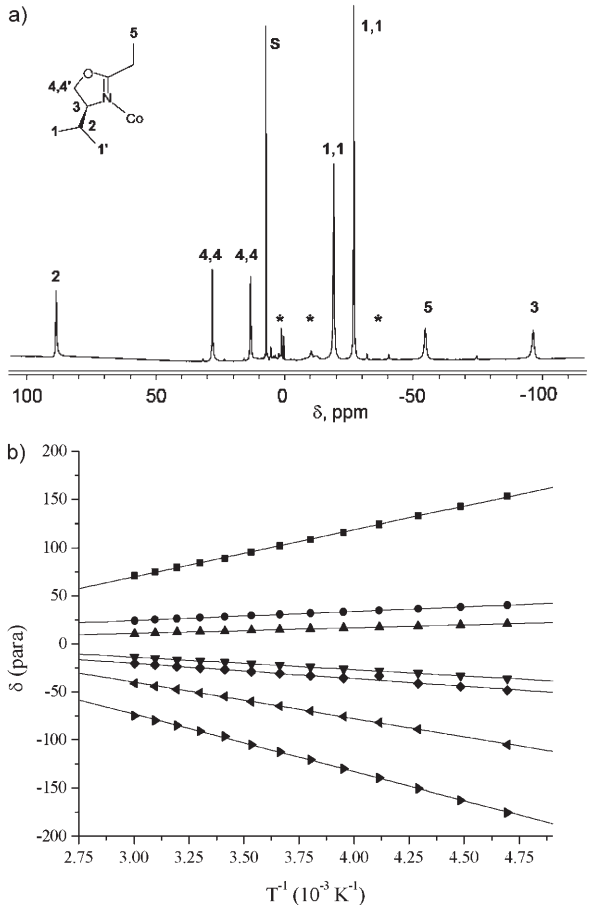

Figure 11. a) ^{1}H NMR spectrum of **10** recorded at 295 K. b) Plot of the paramagnetic shifts of the proton signals in **10** versus 1/T illustrating the Curie behaviour of the molecule in solution at higher temperatures.

shifts of the individual resonances is represented in Figure 11 b. The chemical shifts of the uncoordinated *i*Pr-trisox ligand were used as diamagnetic reference to calculate the $\delta_{para} = \delta_{obs} - \delta_{dia}$ values.

A more systematic study of the magnetic behavior of the dinuclear complexes was carried out using microcrystalline samples of **9**–**11**.

For the Ni_2 complex, **11**, the value of χT at high temperature (2.45 emu K mol^{-1}) corresponds to that expected from the Curie law for a dimer of two Ni^{II} ions with diamagnetic ligands (2.42 emu K mol^{-1}, assuming a g value of 2.20, which is common for octahedral Ni^{II}).[33] At temperatures below 50 K the effects of antiferromagnetic coupling between the two metal centers are clearly visible, leading to a decrease in χT values, which reach 1.1 emu K mol^{-1} at 2 K (Figure 12 a). The magnetic data were fitted with the Heisenberg–Dirac–Van Vleck isotropic model, using the Hamiltonian given in Equation (1):

$$\mathbf{H} = J\,\mathbf{S}_1 \cdot \mathbf{S}_2 \qquad (1)$$

neglecting, in first approximation zero feld splitting (ZFS) effects. The best-fit curve was obtained for $J = 0.83 \pm 0.04$ cm^{-1}, $g = 2.21 \pm 0.02$. Inclusion of ZFS effects has been performed by simulating magnetic data on the basis of the Hamiltonian given in Equation (2):

$$\mathbf{H} = J\,\mathbf{S}_1 \cdot \mathbf{S}_2 \; + \; D(\mathbf{S_{z1}}^2 \; + \mathbf{S_{z2}}^2) \qquad (2)$$

Since the local symmetry of each center is approximately C_3, no rhombic term was included; further, for the sake of simplicity the zero field splitting parameters were considered to be equal for the two metal centers. This approach led to the best agreement with experimental data when $D = 2$ cm^{-1} (which is in the expected range for distorted octahedral Ni^{II}) and $J = 0.83$ cm^{-1}. The magnetic coupling is therefore much weaker than observed, for example, in $[Ni_2(\mu\text{-}Cl_3)(Me_3tacn)_2]^+$, for which an exchange coupling constant

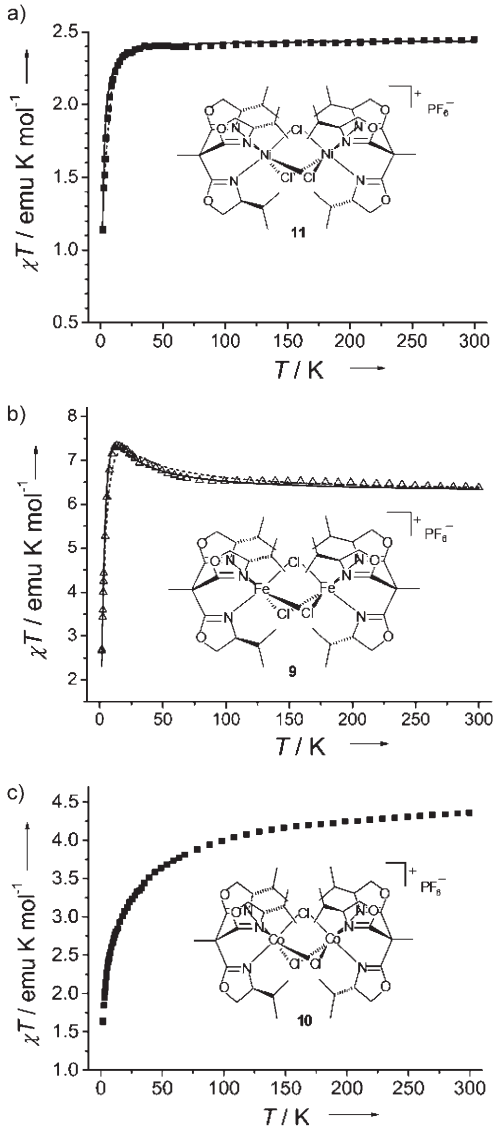

Figure 12. χT versus T plots of microcrystalline samples of complexes **9** (a), **10** (b), and **11a** (c). For complex **9** and **10** dashed and dotted lines are the theoretical curves obtained with and without inclusion of ZFS effects using the parameters reported in the text.

of 21 cm^{-1} has been reported.[23] This difference cannot be attributed to differences in bridging geometry, the average Ni-Cl-Ni bond angles being very similar for both complexes. On the other hand the observed difference might be due to the different donor properties of the trisox ligand (a π donor) compared to Me_3tacn (a simple σ donor) and/or the greater bite angle (N-Ni-N) of the former. Both features are expected to result in a modification of the electron density at the level of the magnetic orbitals.

The room-temperature magnetic data for the iron compound (d^6, high spin), **9**, agree with those expected on the basis of Curie equation (found: 6.38 emu K mol^{-1} expected: 6.30 emu K mol^{-1} if one assumes $g=2.05$), whilst a significant coupling between the magnetic centers is evident below 100 K. The χT curve goes through a maximum at around 15 K and then decreases upon going to lower temperatures (Figure 12b). The increase in χT indicates ferromagnetic coupling, while the decrease in χT below 15 K can be caused either by zero field splitting or by intermolecular antiferromagnetic interactions. The possible presence of intermolecular magnetic interactions has been taken into account using a mean-field approach [Eq. (3)]:[33a]

$$\chi = \frac{\chi_{vv}}{1 + \theta\chi_{vv}} \qquad (3)$$

χ_{vv} being the magnetic susceptibility obtained from the Van Vleck equation resulting from the Hamiltonian (1). With this approach we obtained best-fit values of $J=(-3.0\pm 0.2)$ cm^{-1}, $g=(2.04\pm0.01)$, and $\theta=(0.304\pm0.005)$ cm^{-1}. On the other hand, inclusion of ZFS effects and neglecting intermolecular interactions leads to best simulation parameters of $J=-1.7$ cm^{-1} and $D=10$ cm^{-1}, which is a value within the expected limits for Fe^{II} systems.[33b] Considering the agreement of calculated and experimental curves and the absence of significant intermolecular exchange interaction paths the assumption of large ZFS effects is to be preferred. The observed ferromagnetic coupling is again in qualitative agreement with results reported for the complex $[Fe_2(\mu\text{-}Cl_3)(Me_3tacn)_2]^+$ ($J=-11.6$ cm^{-1}).[23] The smaller coupling constant might again be due to the π-donor properties of the peripheral ligands and/or smaller deviations from ideal molecular C_3 symmetry. Indeed, Wieghardt et al. have shown in detail that a possible ferromagnetic exchange contribution can only be obtained for a ground state with partial 1*e* character (derived from the octahedral t_{2g} state upon lowering the symmetry to C_3). Within this rationale, exact C_3 symmetry results in a pure a_1 electronic ground state, while the π interaction induces a destabilization of the 1*e* orbitals with respect to the a_1 level, both leading to a reduction of the ferromagnetic interaction between the Fe^{II} centers. In this regard, the weaker ferromagnetic coupling, which we observe, may be considered as the result of an electronic structure which is intermediate between that of $[Fe_2(\mu\text{-}Cl_3)(Me_3tacn)_2]^+$, displaying ferromagnetic coupling, and that of $[Fe_2(\mu\text{-}Cl_3)(thf)_6]^+$ featuring a pure a_1 state and three peripheral oxygen donors resulting in weak ($J\approx4$ cm^{-1}) antiferromagnetic coupling.[30,31]

The behavior of the Co^{II} dimer, **10**, (d^7 high spin) is typical for a system with a sizeable orbital contribution as expected for this ion (Figure 12c). The high-temperature value of χT (4.36 emu K mol^{-1}) is in agreement with the presence of two Co^{II} octahedral centers. The observed decrease in the χT curve can not be attributed to intramolecular exchange coupling as depopulation of the highest level resulting from the splitting of the $^4T_{1g}$ state of each single octahedral Co^{II} may strongly contribute to this behavior.[33b] For the same reason it is not possible to analyze the magnetic behavior by using an isotropic spin Hamiltonian.

Finally, if octahedral coordination at metal centers is disfavored, as is the case for the Jahn–Teller-distorted [(*i*Pr-trisox)$CuCl_2$] complex (**12** in Scheme 6), no dinuclear complexes are formed. In this case, the trisox ligand is bidentate (as in the Rh^I complex **7**), which leads to a neutral tetracoordinate copper(II) complex that adopts a characteristic distorted tetrahedral coordination geometry (Figure 13).

The dihedral angle between the N_2Cu and the $CuCl_2$ planes of 40.8° represents an intermediate case between square-planar (0°) and ideal tetrahedral (90°) coordination, frequently referred to as flattened tetrahedral.[34]

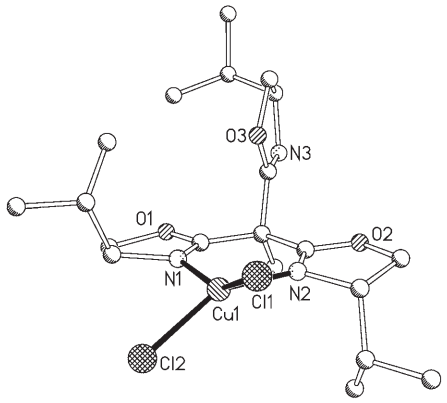

Figure 13. Molecular structure of the copper(II) complex [$CuCl_2$(κ^2-*N*-*i*Pr-trisox)] (**12**). Principal bond lengths [Å] and angles [°]: Cu(1)–Cl(1) 2.2279(5), Cu(1)–Cl(2) 2.2280(5), Cu(1)–N(1) 1.988(2), Cu(1)–N(2) 1.985(2); Cl(1)-Cu(1)-Cl(2) 95.62(2), N(1)-Cu(1)-N(2) 89.15(6), N(1)-Cu(1)-Cl(2) 95.23(5), N(2)-Cu(1)-Cl(1) 94.49(5).

Conclusion

The trisox ligand, which we introduced recently, is the first and thus far only trisoxazoline[35] for which facial coordination to transition metals has been firmly established and which therefore qualifies for the generation of C_3-chiral complexes. The adaptability of the ligand to various types of metal centers has been comprehensively studied in this work. Its modular synthesis aside, the most important point for its application in catalysis is its "non-complementarity" in complexes of the general type $[M(trisox)_2]^{n+}$, if used in enantiomerically pure form. This appears to us to be a pre-

requisite for the use of such tripods as stereodirecting ligands in asymmetric catalytic transformations, in which part of the coordination sphere needs to remain "active".

Experimental Section

All manipulations were performed under an inert atmosphere of dry nitrogen using standard Schlenk techniques or by working in a glove box. THF and diethyl ether were distilled from potassium/benzophenone. Pentane was distilled from a sodium/potassium alloy, dichloromethane was dried over CaH_2 and subsequently distilled. ^1H and ^{13}C NMR spectra were recorded on a Bruker Avance 200, 300, and 400 NMR spectrometers and were referenced by using the residual proton solvent peak (^1H) or carbon resonance (^{13}C). Infrared spectra were obtained on a FT-IR Perkin Elmer 1600 spectrometer. Mass spectra and elemental analyses were recorded by the analytical service of the Heidelberg Chemistry Department or the analytical service of the Strasbourg Chemistry Department. $[Mo(CO)_3(NCMe)_3]$,[36] $[ScCl_3(thf)_3]$,[37] $[RuCl_2(p\text{-cymene})]_2$,[38] $[Rh(cod)_2](BF_4)]$,[39] and $[NiCl_2(PPh_3)_2]$[40] were prepared according to literature procedures. **Caution**: *perchlorates are known to be potentially explosive. These compounds should be handled only on a millimolar scale using appropriate safety precautions.*

Synthesis of the enantiopure trisox ligands: The enantiopure C_3-chiral trisox ligands *i*Pr-trisox(*S*,*S*,*S*) and *t*Bu-trisox(*S*,*S*,*S*) were synthesized as reported previously.[10] The C_1-symmetric cross-coupling product *i*Pr-trisox(*S*,*S*,*R*) was prepared according to an identical procedure with—within experimental error—identical elemental analysis. Spectroscopic data: ^1H NMR ($CDCl_3$, 300 MHz): $\delta = 0.83$–0,92 (m, 18H), 1.72–1.85 (m, 3H), 1.82 (s, 3H), 3.92–4.08 (m, 6H), 4.23–4.33 ppm (m, 3H); ^{13}C NMR ($CDCl_3$, 75 MHz): $\delta = 164.57$,164.51 (C=N), 71.73, 71.68 (*C*H*i*Pr), 70.52 (CH_2), 44.64 ($C_{quat.}$), 32.28, 32.24 ($CH(CH_3)_2$), 21.63 ($CH_{3\,ap.}$), 18.74, 18.49 ($CH(CH_3)(CH_3)$), 17.68, 17.64 ppm ($CH(CH_3)(CH_3)$); MS (EI) : *m/z* (%): 364.2 (62) $[M+1]^+$, 348.2 (9) $[M-CH_3]^+$, 320.2 (33) $[M-CH(CH_3)_2]^+$, 233.1 (100) $[M-C_9H_{22}]^+$.

General synthesis of [Mo(trisox)(CO)$_3$]: A small Schlenk tube was charged with the respective trisox derivative (0.125 mmol) and $[Mo(CO)_6]$ (33.0 mg, 0.125 mmol). Dry acetonitrile (2.0 mL) was then added and the stirred solution was heated at 80°C for 15 h. Evaporation to dryness gave a yellow solid, which upon recrystallisation from CH_2Cl_2/pentane yielded the corresponding molybdenum complex as yellow crystalline solid.

[Mo{*i*Pr-trisox(*S*,*S*,*S*)}(CO)$_3$] (1a): Yield = 60%. ^1H NMR (CD_2Cl_2, 300 MHz): $\delta = 0.71$ (d, $J = 6.9$ Hz, 9H), 0.94 (d, $J = 6.9$ Hz, 9H), 1.68 (s, 3H), 2.72–2.83 (m, 3H), 4.23–4.39 (m, 6H), 4.48 ppm (m, 3H); ^{13}C NMR ($CDCl_3$, 75 MHz): $\delta = 228.1$ (C=O), 166.3 (C=N), 73.3 (*C*H*i*Pr), 70.9 (CH_2), 42.8 ($C_{quat.}$), 29.1 ($CH(CH_3)_2$), 18.4 ($CH(CH_3)(CH_3)$), 13.7 ($CH(CH_3)(CH_3)$) 12.3 ppm (CH_3); IR: $\tilde{\nu} = 1889$ (s), 1852 (s) cm^{-1} (ν(C=O)); MS (FAB+): *m/z* (%): 545.1 (100), 517.2 (32) $[M-CO]^+$.

[Mo{*i*Pr-trisox(*S*,*S*,*R*)}(CO)$_3$] (1b): Yield = 76%. ^1H NMR (CD_2Cl_2, 300 MHz): $\delta = 0.69$ (d, $J = 6.8$ Hz, 2H), 0.79 (d, $J = 6.7$ Hz, 2H), 0.81 (d, $J = 6.7$ Hz, 2H), 0.96 (d, $J = 6.8$ Hz, 2H), 0.98 (d, $J = 7.1$ Hz, 2H), 0.99 (d, $J = 6.8$ Hz, 2H), 1.68 (s, 3H), 2.71–2.87 (m, 3H), 4.18–4.55 ppm (m, 9H); ^{13}C NMR ($CDCl_3$, 75 MHz): $\delta = 228.66$, 227.61, 227.43 (C=O), 167.34, 166.40, 166.25 (C=N), 74.35, 74.25, 73.38 (*C*H*i*Pr), 71.09, 70.71, 70.59 (CH_2), 43.14 ($C_{quat.}$), 29.09, 28.78, 28.75 ($CH(CH_3)_2$), 19.02, 18.98, 18.32 ($CH(CH_3)(CH_3)$), 14.21, 13.79, 13.54 ($CH(CH_3)(CH_3)$) 12.45 ppm (CH_3); IR: $\tilde{\nu} = 1902$ (s), 1890 cm^{-1} (ν(C=O)); MS (EI): *m/z* (%): 545.1 (14) $[M]^+$, 517.1 (8) $[M-CO]^+$, 320.1 (100) $[M-CH(CH_3)_2]^+$.

Synthesis of *rac*-*i*Pr-trisox(C_3) and *rac*-*i*Pr-trisox(C_1): To a solution of 1,1-bis[(4*RS*)-4-isopropyl-4,5-dihydrooxazol-2-yl]ethane (1.1 g, 4.3 mmol of *rac*/*meso* = 1:2) in anhydrous THF (50 mL) was added dropwise *t*BuLi (3.0 mL, 1.7 M in pentane, 5.16 mmol, 1.2 equiv) at −78°C. The resulting yellow solution was stirred for an additional 30 min prior to the addition of 4(*RS*)-2-bromo-4-isopropyloxazoline (1.1 g, 6.1 mmol of the racemic mixture, 1.4 equiv). The solution was then stirred at room temperature for one hour and concentrated to remove the pentane, and finally the Schlenk tube was sealed. The stirred solution was heated for five days at 80°C. The resulting orange solution was evaporated to dryness. The residue was redissolved with dichloromethane (100 mL) and washed with water (10 mL). The aqueous phase was washed with dichloromethane and the organic extract was dried over Na_2SO_4 and concentrated in vacuo to give a yellow oil. A mixture of C_3-symmetric and C_1-symmetric ligands was obtained and could be separated by column chromatography on silica in a 1:3 ratio (EtOAc/MeOH, 98/2) (R_f C_3-symmetric: 0.1; R_f C_1-symmetric ligand: 0.4). Total isolated yield: 51% (C_3: 200 mg collected, C_1: 600 mg collected).

The analytical and NMR spectroscopic data of the C_3 and C_1 racemates are identical to those of the enantiopure ligands (vide supra).

Synthesis of *rac*-[Co(*i*Pr-trisox)(NCMe)$_3$](ClO$_4$)$_2$] (2): A mixture of the *rac*-*i*Pr-trisox (40 mg, 0.11 mmol) and $Co(ClO_4)_2 \cdot 6H_2O$ (19 mg, 0.052 mmol, 0.47 equiv) in acetonitrile (2 mL) was stirred for half an hour at room temperature. The solvent was removed in vacuo and the resulting pale pink solid was washed twice with diethyl ether to yield **2** in quantitative yield. Suitable crystals for X-ray diffraction were obtained from acetonitrile/diethyl ether. MS (FAB+): *m/z* (%): 521.4 $[(trisox)Co(ClO_4)]^+$ (100); IR: $\tilde{\nu} = 2315.5$ (s), 2284.4 (s), 2272.1 (s), 2020.7 (m), 2015.6 (m) cm^{-1}; UV/Vis: $\lambda = 500$ nm ($\varepsilon = 36$; LF-transition corresponding to $^4T_{1g}(F) \rightarrow {}^4T_{1g}(P)$ in the octahedral reference system); elemental analysis (%) calcd for $C_{26}H_{42}Cl_2CoN_6O_{11}(3H_2O)$: C 39.11, H 6.06, N 10.52; found: C 39.14, H 5.59, N 9.29.

Synthesis of [Co{*i*Pr-trisox(*S*,*S*,*S*)}{*i*Pr-trisox(*R*,*R*,*R*)}](ClO$_4$)$_2$ (3): A mixture of the *rac*-*i*Pr-trisox (20 mg, 0.055 mmol) and $Co(ClO_4)_2 \cdot 6H_2O$ (10 mg, 0.027 mmol, 0.50 equiv) in dichloromethane (2 mL) was stirred for 1 h at room temperature. The solvent was removed in vacuo and the resulting light pink solid was washed twice with diethyl ether to yield **3** in quantitative yield. MS (FAB+): *m/z* (%): 785.5 $[(trisox)_2Co]^+$ (15), 673.4 $[(trisox)_2Co\text{-}(C_6H_{10}NO)]^+$ (30), 521.2 $[(trisox)Co(ClO_4)]^+$ (100); UV/Vis: $\lambda = 549$ nm ($\varepsilon = 40$; LF-transition corresponding to $^4T_{1g}(F) \rightarrow {}^4T_{1g}(P)$ in the octahedral reference system); elemental analysis (%) calcd for $C_{40}H_{66}Cl_2CoN_6O_{14}(6H_2O)$: C 43.96, H 7.19, N 7.69; found: C 44.18, H 6.82, N 7.40.

Synthesis of [ScCl$_3$(*i*Pr-trisox)] (4): To a stirred suspension of $[ScCl_3(thf)_3]$ (131 mg, 0.358 mmol) in THF (10 mL) was added a solution of *i*Pr-trisox (130 mg, 0.358 mmol) in THF (10 mL). The reaction mixture was stirred for 18 h, before the volatiles were removed under reduced pressure to afford $[ScCl_3(i\text{Pr-trisox})]$ in 84% yield (155 mg). ^1H NMR (CD_2Cl_2, 300.1 MHz, 293 K): $\delta = 4.90$ (td, $^3J = 8.7$ Hz, $^3J = 3.6$ Hz, 3H, C*H*iPr), 4.51 (m, 6H, CH_2), 2.89 (sept d, $^3J = 7.0$ Hz, $^3J = 3.6$ Hz, 3H, C*H*Me$_2$), 1.73 (s, 3H, Me$_{apical}$), 0.89 (d, $^3J = 7.2$ Hz, 9H, CH*Me*$_2$), 0.71 ppm (d, $^3J = 6.8$ Hzm, 9H, CH*Me*$_2$); $^{13}C\{^1H\}$ NMR (CD_2Cl_2, 75.5 MHz, 293 K): $\delta = 169.5$ (C=N), 72.6 (CH_2), 72.0 (*C*H*i*Pr), 44.3 (*C*Me$_{apical}$), 28.5 (*C*HMe$_2$), 18.9 (CH*Me*$_2$), 14.3 (CH*Me*$_2$), 12.7 ppm (Me$_{apical}$).

Synthesis of [Fe(*i*Pr-trisox)(NCMe)$_3$](BF$_4$)$_2$ (5): Under a nitrogen atmosphere, a small Schlenk tube was charged with the trisox-*t*Bu ligand (101.5 mg, 0.25 mmol) and anhydrous $FeCl_2$ (31.7 mg, 0.25 mmol). Dry acetonitrile (1.5 mL) was added and the solution was stirred at 35°C until the complete dissolution of the white solid (ca. 2 h). Solid $AgBF_4$ (98.0 mg, 0.50 mmol) was then added and the resulting mixture was stirred overnight at room temperature (the flask was covered with aluminum foil to protect the silver salts from light). The solution was filtered over Celite, and the solid was washed with acetonitrile. The solution was then concentrated and layered with diethyl ether. Colorless crystals were isolated after 24 h (suitable for X-ray analysis) and dried under vacuum to give compound **5** (112 mg, 0.15 mmol; 60%). IR (nujol): $\tilde{\nu} = 2270$, 2288 cm^{-1} (m, $\nu_{(C\equiv N)}$); elemental analysis (%) calcd for $C_{29}H_{48}N_6O_3B_2F_8Fe$: C 45.89, H 6.38; found: C 46.08, H 6.56.

Synthesis of [Ru(η^6-*p*-cymene)(*i*Pr-trisox)](PF$_6$)$_2$ (6): In a Schlenk tube were placed together the *i*Pr-trisox ligand (25 mg, 0.069 mmol) and $[RuCl_2(p\text{-cymene})]_2$ (21 mg, 0.034 mmol) in dry CH_2Cl_2 (10 mL). The orange solution formed was stirred at room temperature for 1 h. After that time, $AgPF_6$ (35 mg, 0.137 mmol) was added and a white solid immediately was observed. The suspension was stirred at room temperature for 3 h and filtered through Celite. The solution obtained was concentrat-

ed under high pressure, and the red oil obtained was washed twice with pentane to give the desired complex as an orange crystalline solid (49 mg, 78% yield). Suitable crystals for X-ray diffraction studies were obtained by slow diffusion of Et_2O in a solution of the complex in CH_2Cl_2. ^{1}H NMR (CD_2Cl_2, 400 MHz): $\delta = 0.635$ (d, $^3J_{H,H} = 5.1$ Hz, 9H, $CH(CH_3)(CH_3)$), 0.137 (d, $^3J_{H,H} = 5.1$ Hz, 9H, $CH(CH_3)(CH_3)$), 1.36 (d, $^3J_{H,H} = 1.5$ Hz, 3H, $(CH_3)_2CHC_6H_4(CH_3)$-*p*), 1.37 (d, $^3J_{H,H} = 1.5$ Hz, 3H, $(CH_3)_2CHC_6H_4(CH_3)$-*p*), 1.63 (s, 3H, CH_3), 2.22 (m, 3H, $CH(CH_3)_2$), 2.45 (s, 3H, $(CH_3)_2CHC_6H_4(CH_3)$-*p*), 2.85 (m, 1H, $(CH_3)_2CHC_6H_4(CH_3)$-*p*), 4.72, 4.75, 4.77 (s, 3H, CH_{oxa}), 4.81–4.83 (m, 3H, CH_{2oxa}), 4.91–4.94 (dd,, $^2J_{H,H} = 7.2$ Hz, $^3J_{H,H} = 2.1$ Hz, 3H, CH_{2oxa}), 6.26, 6.13, 6.09, 5.99 ppm (d, 4H, $(CH_3)_2CHC_6H_4(CH_3)$-*p*); ^{13}C{^{1}H} (CD_2Cl_2, 400 MHz): $\delta = 170.5$ (3C, NCO), 117.8, 108.5 (2C, $C_{p\text{-cymene}}$), 91.3, 89.4, 81.1, 79.9 (4C, $CH_{p\text{-cymene}}$), 76.2 (3C, CH_{oxa}), 74.9 (3C, CH_{2oxa}), 44.7 (1C, $C_{quat.}$), 33.9 (1C, $(CH_3)_2CHC_6H_4(CH_3)$-*p*), 31.4 (3C, $CH(CH_3)_3$), 26.0 (1C, $(CH_3)_2CHC_6H_4(CH_3)$-*p*), 24.1, 21.6 (2C, $(CH_3)_2CHC_6H_4(CH_3)$-*p*), 19.2 (3C, $CH(CH_3)(CH_3)$), 15.2 (3C, $CH(CH_3)(CH_3)$), 12.6 ppm (CH_3); elemental analysis (%) calcd for $C_{30}H_{47}N_3O_3RuP_2F_{12}$ (889.711): C 40.54, H 5.33, N 4.73; found: C 40.38, H 5.22, N 4.86. MS (FAB) *m/z* (%): 618.3 (89) [(*trisox*)Ru(*p*-cymene)F]$^+$, 599.3 (51) [(*trisox*)Ru(*p*-cymene)]$^+$, 487.3 (20) [(*trisox*)Ru(*p*-cymene)]$^+$.

Synthesis of [Rh(*i*Pr-trisox)(cod)]BF_4 (7): A mixture of *i*Pr-trisox (100 mg, 0.275 mmol) and $[Rh(cod)_2BF_4]$ (106 mg, 0.262 mmol) in dichloromethane (5 mL) was stirred under nitrogen for one hour. The solvent was removed in vacuo and the resulting yellow solid was washed several times with diethyl ether to yield an orange powder (130 mg, 0.196 mmol), 71%. Single crystals of **7** suitable for X-ray diffraction were formed by slow diffusion of a solution of the complex in THF and diethyl ether. ^{1}H NMR (CD_2Cl_2, 300 MHz): $\delta = 0.82$ (d, $J = 6.8$ Hz, $9H_{oxa}$), 0.94 (d, $J = 6.9$ Hz, $9H_{oxa}$), 1.54–1.56 (m, $3H_{oxa}$ + $CH_{2[cod]}$), 1.79 (s, $3H_{oxa}$), 1.98–2.1 (m broad, $CH_{2[cod]}$), 2.22–2.36 (m, $CH_{2[cod]}$), 2.47–2.62 (m, $CH_{2[cod]}$), 4–4.07 (m, $3H_{oxa}$), 4.11–4.20 (m, $CH_{[cod]}$), 4.31–4.46 ppm (m, $6H_{oxa}$ + $CH_{[cod]}$); ^{13}C NMR: $\delta = 167.7$ (C=N), 83.8 ($CH_{[cod]}$), 83.7 ($CH_{[cod]}$), 80.2 ($CH_{[cod]}$), 80.0 ($CH_{[cod]}$), 71.6 (CH_2), 70.9 (CHiPr), 45.7 ($C_{quat.}$), 31.5 ($CH(CH_3)_2$), 31.3($CH_{2[cod]}$), 29.3 ($CH_{2[cod]}$), 18.3 ($CH(CH_3)(CH_3)$), 15.3 ($CH(CH_3)(CH_3)$), 12.9 ppm (CH_3); MS (FAB): *m/z* (%): 574.4 $[M]^+$(100), 470.2 $[M-\text{cod}]^+$(19); IR: $\tilde{\nu} = 1664.0$, 1643.4, 1622.8 cm^{-1} (C=N).

Synthesis of [$RhBr_3$(*i*Pr-trisox)] (8): A solution of **7** (130 mg, 0.196 mmol) in THF (10 mL) was cooled down to −78°C. One equivalent of $CsBr_3$ (73 mg, 0.196 mmol) was then added and the solution was allowed to warm up slowly for 12 h. This resulted in the formation of a red solution and a precipitate. The solvent was evaporated in vacuo and the resulting red solid was extracted with toluene. It was filtered through Celite under an inert gas atmosphere and the solvent evaporated in vacuo. The desired product was washed several times with diethyl ether to give 20 mg (15%, 0.028 mmol) of **8** as a pale red solid. The same reaction was carried out in CH_2Cl_2 and toluene and gave 30% and 44% yield, respectively. Single crystals of **2** suitable for X-ray diffraction were formed by slow diffusion of a solution of the complex in THF and diethyl ether. ^{1}H NMR (CD_2Cl_2, 300 MHz): $\delta = 0.62$ (d, $J = 6.6$ Hz, 9H), 0.84 (d, $J = 7.1$ Hz, 9H), 1.75 (s, 3H), 3.20 (m, 3H), 4.56–4.71 (m, 6H), 5.15 ppm (m, 3H); ^{13}C NMR: $\delta = 166.2$ (C=N), 73.4 (CHiPr), 69.2 (CH_2), 27.6 ($CH(CH_3)_2$), 27.4 ($C_{quat.}$), 18.1 ($CH(CH_3)(CH_3)$), 14.3 ($CH(CH_3)(CH_3)$), 11.2 ppm (CH_3); MS (FAB): *m/z* (%): 704.5 $[M]^+$(16), 625.6 $[M-\text{Br}+\text{H}]^+$(100); elemental analysis (%) calcd for $C_{20}H_{33}Br_3N_3O_3Rh$ (702.91): C 34.02, H 4.71, N 5.95; found: C 34.24, H 4.68, N 5.89.

Synthesis of [Fe_2(μ-Cl_3)(*i*Pr-trisox)$_2$]PF_6 (9): To a solution of *i*Pr-trisox (100 mg, 0.275 mmol) in methanol (4 mL) was added anhydrous $FeCl_2$ (31 mg, 0.245 mmol), and the resulting suspension was stirred for 10 min. Then KPF_6 (50 mg, 0.272 mmol) was added and the mixture was stirred 2 h at 50°C and overnight at room temperature. After removal of the solvent in vacuum, the residue was suspended in dichloromethane and filtered. The solvent was evaporated and the residue was washed twice with diethyl ether to yield the title complex as an almost colorless powder which was dried in a vacuum (101 mg, 66%). Crystals suitable for X-ray analysis were prepared by slow vapor phase diffusion of diethyl ether into a dichloromethane solution of the complex. MS (FAB+): *m/z*: 945.3 ($[M^+]$), 454.2 ($[L_3FeCl^+]$); elemental analysis (%) calcd for $C_{41}H_{68}Cl_5F_6Fe_2O_6P$ ($[(L_3)_2Fe_2(\mu\text{-}Cl_3)]PF_6 \cdot CH_2Cl_2$): C 41.91, H 5.83, N 7.15; found: C 42.22, H 6.01, N 6.82.

Synthesis of [Co_2(μ-Cl_3)(*i*Pr-trisox)$_2$]PF_6 (10). To a solution of *i*Pr-trisox (54 mg, 0.149 mmol) in methanol (2.5 mL) was added anhydrous $CoCl_2 \cdot 6H_2O$ (32 mg, 134 mmol), and the resulting suspension was stirred for 10 min. Then KPF_6 (37 mg, 0.201 mmol) was added and the mixture was stirred for 2 h at 50°C and overnight at room temperature. After removal of the solvent in vacuum, the residue was suspended in dichloromethane and filtered. The solvent was evaporated and the residue was washed twice with hexane to yield the title complex as a deep blue powder which was dried under vacuum (73 mg, 71%). Crystals suitable for X-ray analysis were prepared by slow diffusion of hexane into a dichloromethane solution of the complex. MS (FAB+): *m/z*: 949.3 ($[M^+]$); 457.2 ($[L_3CoCl]^+$, 100); elemental analysis (%) calcd for $C_{40}H_{66}Cl_3F_6Co_2O_6P$: C 43.83, H 6.07, N 7.67; found: C 43.96, H 6.17, N 7.39.

Synthesis of [Ni_2(μ-Cl_3)(*i*Pr-trisox)$_2$]PF_6 (11): To a solution of *i*Pr-trisox (86 mg, 0.237 mmol) in ethanol (4 mL) was added $NiCl_2 \cdot 6H_2O$ (51 mg, 0.215 mmol), and the resulting suspension was stirred for 10 min. Then KPF_6 (60 mg, 0.326 mmol) was added and the mixture was stirred 4 h at 70°C. After the mixture was cooled to room temperature, the solvent was removed in vacuo, the residue was suspended in tetrahydrofuran (5 mL) and filtered. Upon slow evaporation of the solvent the title complex precipitated as green crystals (117 mg, 79%). Crystals suitable for X-ray analysis were prepared by slow diffusion of diethyl ether vapors into a dichloromethane solution of the complex. MS (FAB+): *m/z*: 950.2 ($[M]^+$), 587.6 ($[M-L_3]^+$), 456.4 ($[i\text{Pr-trisoxNiCl}^+]$, 100); elemental analysis (%) calcd for $C_{41}H_{68}Cl_5F_6Ni_2O_6P$ ($[(L_3)_2Ni_2(\mu\text{-}Cl_3)]PF_6 \cdot CH_2Cl_2$): C 41.91, H 5.63, N 7.06; found: C 42.22, H 5.81, N 6.92.

Synthesis of [$CuCl_2$(*i*Pr-trisox)] (12): To a solution of *i*Pr-trisox (99 mg, 0.27 mmol) in dichloromethane (1 mL) was added anhydrous $CuCl_2$ (33 mg, 0.25 mmol), and the suspension was stirred for 1 h. The resulting green solution was layered with diethyl ether (5 mL), green crystals of the title compound were obtained overnight. The solvents were removed by cannula and the product was dried in a vacuum (110 mg, 88%). MS (FAB+): *m/z*: 496.1 ($[M^+]$), 460.6 ($(i\text{Pr-trisoxCuCl}^+]$); elemental analysis (%) calcd for $C_{20}H_{33}Cl_2CuN_3O_3$ ($[(L_3)CuCl_2]$): C 48.24, H 6.68, N 8.44; found: C 48.00, H 6.74, N 8.28.

Magnetic measurements and analysis of the data: The magnetic susceptibilities of the powdered samples were measured with a Cryogenic SQUID S600 magnetometer in a temperature range of 2 to 300 K and with an applied field of 1.0 T. The diamagnetic contribution affecting the resulting data was corrected with the Pascal's constants. Simulations of χT versus T curves with inclusion of exchange coupling and zero field splitting effects were performed using the Magpack Routine.[41]

Crystal structure determinations: Suitable crystals of ***i*Pr-trisox(*rac*-C_3)** and of the complexes **1a**, **1b**, **2**, **4**, **5**, **6**, **7**, **8**, **9**, **10**, **11**, **11a**, and **12** were obtained by layering concentrated solutions in polar solvents with pentane or diethyl ether and allowing slow diffusion at room temperature. Intensity data were collected at low temperature on Nonius Kappa CCD (***i*Pr-trisox(*rac*-C_3)**, **1a**, **1b**, **2**, **4**, **5**, **6**, **7**, **8**) and Bruker Smart 1000 CCD (**9**, **10**, **11**, **11a**, and **12**) diffractometers. The structures were solved by using direct methods with absorption corrections being applied as part of the data scaling procedure. After refinement of the heavy atoms, difference Fourier maps revealed the maxima of residual electron density close to the positions expected for the hydrogen atoms. They were introduced as fixed contributors in the structure factor calculations and treated with a riding model, with isotropic temperature factors but not refined. A final difference map revealed no significant maxima of residual electron density. Structure solution and refinement were performed by using the programs OpenMoleN,[42] SHELXS-86,[43] SHELXL-97,[44] or CRYSTALS.[45] Graphical representations were drawn with PLATON.[46] Crystal data and experimental details are given in Table 2.

CCDC-627150–CCDC-627163 contain the supplementary crystallographic data for this paper. These data can be obtained free of charge from the Cambridge Crystallographic Data Centre via www.ccdc.cam.ac.uk/data_request/cif.

Table 2. X-ray experimental data of the crystallographically characterized compounds.

	***i*Pr-trisox-*rac*-C_3**	**1a**	**1b**	**2**	**4**
empirical formula	$C_{20}H_{33}N_3O_3$	$C_{23}H_{33}Mo\ N_3O_6$	$C_{23}H_{33}MoN_3O_6$	$C_{26}H_{42}Cl_2CoN_6O_{11}$	$C_{20}H_{33}Cl_3N_3O_3Sc$
formula weight	363.49	543.46	543.46	744.49	514.81
crystal size [mm]	0.20×0.15×0.10	0.20×0.10×0.05	0.10×0.08×0.07	0.10×0.10×0.10	0.20×0.12×0.10
crystal system	triclinic	orthorhombic	orthorhombic	monoclinic	monoclinic
space group	$P\bar{1}$	$P2_12_12_1$	$P2_12_12_1$	$P2_1/n$	$P2_1$
a [Å]	10.1130(2)	7.916(5)	9.0170(10)	18.626(5)	8.1013(10)
b [Å]	10.2640(2)	9.290(5)	16.192(2)	10.915(3)	9.2858(10)
c [Å]	11.8750(5)	34.774(5)	34.097(5)	34.540(9)	17.0061(10)
α [°]	92.8740(9)	90	90	90	90
β [°]	106.2990(10)	90	90	90.81(5)	94.023(10)
γ [°]	117.6360(16)	90	90	90	90
V [Å^3]	1024.27(5)	2557(2)	4978.3(11)	7021(3)	1276.2(2)
Z	2	4	8	8	2
ρ_{calcd} [Mgm^{-3}]	1.179	1.412	1.450	1.409	1.340
μ [mm^{-1}]	0.079	0.554	0.569	0.703	0.627
max., min. trans.	n.d.	n.d.	n.d.	n.d.	0.9392, 0.9275
index ranges, *hkl*	−13 to 14, −14 to 14, −16 to 12	0 to 11, 0 to 13, −48 to 48	0 to 11, 0 to 20, −44 to 44	−24 to 26, −15 to 14, −48 to 48	−11 to 11, −11 to 13, −23 to 23
θ [°]	2.4 to 30.0	2.3 to 30.0	1.4 to 27.5	2.1 to 30.0	1.2 to 30.0
T [K]	173(2)	173(2)	173(2)	173(2)	173(2)
F(000)	396	1128	2256	3112	540
refl. collected	8023	20538	175036	90368	
refl. indep. [R_{int}]	5968 [0.0251]	6729	9536	20449 [0.0525]	5608
data/rest./par.	5968/0/235	6729/0/298	9535/0/595	20449/0/829	4090/1/272
GOF on F^2	1.027	0.932	0.921	0.986	1.030
final R indices [$I>2\sigma(I)$]					
R_1, wR_2	0.0559, 0.1151	0.0348, 0.0729	0.0611, 0.1051	0.0552, 0.1400	0.0357, 0.0359
R indices (all data)					
R_1, wR_2	0.1011, 0.1322	0.0520, 0.0804	0.1324, 0.1226	0.1003, 0.1603	0.0614, 0.0453
abs. structural par.		−0.03(3)	−0.03(5)		−0.02(3)
largest res. [e Å^{-3}]	0.243 and −0.206	0.765 and −0.915	1.142 and −0.718	1.001 and −0.628	0.29 and −0.37

	5	**6**	**7**	**8**	**9**
empirical formula	$C_{31}H_{51}B_2F_8FeN_7O_3$	$C_{30}H_{47}F_{12}N_3O_3P_2Ru$	$C_{28}H_{45}BF_4N_3O_3Rh$	$C_{20}H_{33}Br_3N_3O_3Rh$	$C_{41}H_{68}Cl_5F_6Fe_2N_6O_6P$
formula weight	799.26	888.72	661.40	706.14	1174.96
crystal size [mm]	0.13×0.10×0.08	0.08×0.07×0.05	0.08×0.06×0.06	0.14×0.14×0.10	0.20×0.20×0.16
crystal system	triclinic	monoclinic	hexagonal	monoclinic	orthorhombic
space group	$P1$	$P2_1$	$P3_221$	$P2_1$	$P2_12_12_1$
a [Å]	10.132(5)	10.503(3)	11.2197(2)	8.1691(2)	12.6983(2)
b [Å]	10.446(5)	19.947(5)	11.2197(2)	9.3111(2)	17.9556(2)
c [Å]	10.692(5)	17.635(6)	43.1788(9)	16.9366(5)	24.6894(4)
α [°]	75.586(5)	90	90	90	90
β [°]	70.467(5)	90.22(3)	90	94.0037(10)	90
γ [°]	79.200(5)	90	120	90	90
V [Å^3]	1026.2(9)	3694.6(19)	4707.2(2)	1285.11(6)	5629.3(1)
Z	1	4	6	2	4
ρ_{calcd} [Mgm^{-3}]	1.293	1.598	1.400	1.82	1.390
μ [mm^{-1}]	0.442	0.607	0.600	5.353	0.847
max.,min. trans.	n.d.	n.d.	n.d.	0.585, 0.485	1.0000, 0.8200
index ranges, *hkl*	−15 to 16, −16 to 16, −17 to 16	0 to 13, 0 to 22, −21 to 22	−14 to 14, −11 to 11, −50 to 47	−11 to 11, −13 to 11, −23 to 23	−17 to 17, −25 to 25, −34 to 34
θ [°]	2.0 to 35.0	2.5 to 26.4	2.5 to 27.5	2.5 to 30.0	2.5 to 30.0
T [K]	173(2)	173(2)	173(2)	173(2)	173(2)
F(000)	418	1816	2064	696	2440
refl. collected	23269	10892	11434		
refl. indep. [R_{int}]	14028 [0.0296]	7234	6192 [0.050]	6654 [0.050]	15637 [0.040]
data/rest./par.	14028/3/469	7234/1/901	2437/3/324	5335/1/270	8849/0/604
GOF on F^2	1.037	1.048	1.002	1.134	1.788
final R indices [$I>2\sigma(I)$]					
R_1, wR_2	0.0499, 0.1228	0.0599, 0.1233	0.071, 0.087	0.031, 0.036	0.074, 0.085
R indices (all data)					
R_1, wR_2	0.0588, 0.1293	0.1090, 0.1422	0.105, 0.174	0.047, 0.075	0.136, 0.232
abs. structural par.	0.015(8)	0.06(5)	0.1(1)	0.00(1)	0.07(2)
largest res. [e Å^{-3}]	0.581 and −0.400	0.977 and −0.738	1.241 and −1.290	0.757 and −0.369	1.881 and −1.295

	10	**11**	**11a**	**12**
empirical formula	$C_{42}H_{70}Cl_7Co_2F_6N_6O_6P$	$C_{40}H_{66}Cl_3F_6N_6Ni_2O_6P$	$C_{15.33}H_{28}Cl_{1.33}N_2Ni_{0.67}O_3$	$C_{20}H_{33}Cl_2CuN_3O_3$
formula weight	1266.06	1095.74	374.75	497.93
crystal size [mm]	0.20×0.18×0.12	0.20×0.10×0.10	0.20×0.10×0.10	0.30×0.18×0.12
crystal system	orthorhombic	orthorhombic	cubic	orthorhombic
space group	$P2_12_12_1$	$C222_1$	$P2_13$	$P2_12_12_1$
a [Å]	13.0696(1)	23.850(5)	17.863(5)	9.7255(4)
b [Å]	17.8771(2)	25.400(5)	17.863(5)	12.7360(5)
c [Å]	24.6966(3)	20.181(5)	17.863(5)	19.0667(8)
α [°]	90	90	90	90
β [°]	90	90	90	90
γ [°]	90	90	90	90
V [Å^3]	5770.3(1)	12226(5)	5700(3)	2361.68(17)
Z	4	8	12	4
ρ_{calcd} [Mgm^{-3}]	1.460	1.191	1.310	1.400
μ [mm^{-1}]	0.993	0.831	0.901	1.176
max., min. trans.	0.8910, 0.8266	0.925, 0.911	0.9139, 0.9139	1.000, 0.851
index ranges, hkl	−18 to 18, −25 to 25, −34 to 34	−33 to 33, 0 to 35, 0 to 28	−25 to 25, −17 to 17, −17 to 17	−14 to 14, 0 to 18, 0 to 28
θ [°]	2.5 to 30.0	1.2 to 30.0	1.6 to 30.0	1.9 to 32.0
T [K]	173(2)	173(2)	173(2)	173(2)
F(000)	2616	4576	2391.612	1044
refl. collected				22756
refl. indep. [R_{int}]	16667 [0.040]	17801	5428	8019 [0.0376]
data/rest./par.	10759/0/631	17748/27/580	3350/63/245	8019/0/394
GOF on F^2	1.792	0.9115	1.1022	1.065
final R indices [$I>2\sigma(I)$]				
R_1, wR_2	0.064, 0.080	0.0592, 0.1418	0.0387, 0.0334	0.0316, 0.0712
R indices (all data)				
R_1, wR_2	0.104, 0.161	0.0784, 0.1523	0.0807, 0.0656	0.0399, 0.0765
abs. structural par.	−0.01(2)	0.014(3)	0.007(17)	−0.002(8)
largest res. [e Å^{-3}]	1.704 and −1.268	0.01 and −0.02	0.44 and −0.40	0.436 and −0.292

Computational details: All calculations were performed by using the Gaussian 03 program.[47] All calculated structures were optimized without geometry constraints, with each optimization being followed by a frequency calculation (for quantum-mechanical calculations) to confirm the nature of the located extrema (minimum or transition state). Where possible, molecular parameters of optimized structures were compared to available X-ray data and exhibited no significant differences. For ONIOM calculations involving the *i*Pr-trisox ligand, the trisox isopropyl groups and apical methyl group were calculated at the UFF level, with the remainder of the molecule calculated with the B3PW91 method.

The structures of the cobalt complexes $[Co(i\text{Pr-trisox})_2]^{2+}$ and $[Co_2(i\text{Pr-trisox})_2Cl_3]^-$ were calculated by using molecular mechanics (UFF). DFT or ONIOM (QM/MM) calculations failed to converge to satisfactory minima, presumably to the large size of the molecules involved, therefore the corresponding zinc complexes $[Zn(i\text{Pr-trisox})_2]^{2+}$ and $[Zn_2(i\text{Pr-trisox})_2Cl_3]^+$ were calculated using ONIOM methodology, using 6–31G(d,p) for the metal and coordinating atoms, and 6–31G for the remaining centers. For the mononuclear systems, the *SSS-RRR* complex converged satisfactorily and confirms the validity of the MM models, whereas the *SSS-SSS* isomer failed to reach a satisfactory minimum on the potential energy surface.

Acknowledgements

We thank the Deutsche Forschungsgemeinschaft (SFB 623), the Fonds der Chemischen Industrie (Germany), the CNRS (France) and the Institut Universitaire de France for support of this work and the Ministère de l'Education Nationale de la Recherche et de la Technologie for a Ph.D. grant to C.D. Support by BASF (Ludwigshafen) and Degussa (Hanau) is gratefully acknowledged. We also thank Prof. R. Welter, Dr. A. DeCian and N. Gruber for the X-ray diffraction studies. Finally, L. S. and G. P. acknowledge financial support of MIUR.

[1] a) C. Moberg, *Angew. Chem.* **1998**, *110*, 260; *Angew. Chem. Int. Ed.* **1998**, *37*, 248; b) M. C. Keyes, W. B. Tolman, *Adv. Cat. Proc.* **1997**, *2*, 189.

[2] a) S. E. Gibson, M. P. Castaldi, *Chem. Commun.* **2006**, 3045; b) S. E. Gibson, M. P. Castaldi, *Angew. Chem.* **2006**, *118*, 4834; *Angew. Chem. Int. Ed.* **2006**, *45*, 4718; c) C. Moberg, *Angew. Chem.* **2006**, *118*, 4838; *Angew. Chem. Int. Ed.* **2006**, *45*, 4721.

[3] Examples of the use of C_3-chiral ligands in asymmetric catalysis: a) H. Brunner, A. F. M. M. Rahman, *Chem. Ber.* **1984**, *117*, 710; b) M. J. Burk, R. L. Harlow, *Angew. Chem.* **1990**, *102*, 1511; *Angew. Chem. Int. Ed. Engl.* **1990**, *29*, 1467; c) M. J. Burk, J. E. Feaster, R. L. Harlow, *Tetrahedron: Asymmetry* **1991**, *2*, 569; d) T. R. Ward, L. M. Venanzi, A. Albinati, F. Lianza, T. Gerfin, V. Gramlich, G. M. R. Tombo, *Helv. Chim. Acta* **1991**, *74*, 983; e) M. J. Baker, P. J. Pringle, *J. Chem. Soc. Chem. Commun.* **1993**, 314; f) H. Adolfsson, K. Wärnmark, C. Moberg, *J. Chem. Soc. Chem. Commun.* **1992**, 1054; g) H. Adolfsson, K. Nordström, K. Wärnmark, C. Moberg, *Tetrahedron: Asymmetry* **1996**, *7*, 1967; h) D. D. LeCloux, W. B. Tolman, *J. Am. Chem. Soc.* **1993**, *115*, 1153; i) C. J. Tokar, P. B. Kettler, W. B. Tolman, *Organometallics* **1992**, *11*, 2737; j) D. D. Lecloux, C. J. Tokar, M. Osawa, R. P. Houser, M. C. Keyes, W. B. Tolman, *Organometallics* **1994**, *13*, 2855; k) K. Kawasaki, S. Tsumura, T. Katsuki, *Synlett.* **1995**, 1245.

[4] Asymmetric catalysis with chiral aminoalcohols as ligands: a) W. A. Nugent, R. L. Harlow, *J. Am. Chem. Soc.* **1994**, *116*, 6142; b) F. DiFuria, G. Licini, G. Modena, R. Motterle, W. A. Nugent, *J. Org. Chem.* **1996**, *61*, 5175; c) H. Lütjens, P. Knochel, *Tetrahedron: Asymmetry* **1994**, *5*, 1161; d) H. Lütjens, G. Wahl, F. Möller, F. Knochel, J. Sundermeyer, *Organometallics* **1997**, *16*, 5869; e) M. Cernerud, H. Adolfsson, C. Moberg, *Tetrahedron: Asymmetry* **1997**, *8*, 2655; f) W. A. Nugent, G. Licini, M. Bonchio, O. Bortolini, M. G. Finn, B. W. McCleland, *Pure Appl. Chem.* **1998**, *70*, 1041; g) M. Bonchio, G. Licini, F. Di Furia, S. Mantovani, G. Modena, W. A. Nugent, *J. Org. Chem.* **1999**, *64*, 1326; h) M. Bonchio, G. Licini, G. Modena, O.

Bortolini, S. Moro, W. A. Nugent, *J. Am. Chem. Soc.* **1999**, *121*, 6258; i) M. Bonchio, O. Bortolini, G. Licini, S. Moro, W. A. Nugent, *Eur. J. Org. Chem.* **2003**, 507; j) M. G. Buonomenna, E. Drioli, W. A. Nugent, L. J. Prins, P. Scrimin, G. Licini, *Tetrahedron Lett.* **2004**, *45*, 7515.

[5] Recent advances in the design of C_3-chiral podands: a) G. Bringmann, M. Breuning, R.-M. Pfeifer, P. Schreiber, *Tetrahedron: Asymmetry* **2003**, *14*, 2225; b) G. Bringmann, R.-M. Pfeifer, C. Rummey, K. Hartner, M. Breuning, *J. Org. Chem.* **2003**, *68*, 6859; c) T. Fang, D.-M- Du, S.-F. Lu, J. Xu, *Org. Lett.* **2005**, *7*, 2081; d) M. P. Castaldi, S. E. Gibson, M. Rudd, A. J. P. White, *Angew. Chem.* **2005**, *117*, 3498; *Angew. Chem. Int. Ed.* **2005**, *44*, 3432; e) M. P. Castaldi, S. E. Gibson, M. Rudd, A. J. P. White, *Chem. Eur. J.* **2005**, *11*, 138.

[6] H. B. Kagan, T.-P. Dang, *J. Am. Chem. Soc.* **1972**, *94*, 6429.

[7] A. von Zelewsky, *Stereochemistry of Coordination Compounds*, Wiley, Chichester, **1996**.

[8] For a discussion of the special case of five-coordinate complexes bearing C_3-chiral tripods, see: L. H. Gade, P. Renner, H. Memmler, F. Fecher, C. H. Galka, M. Laubender, S. Radojevic, M. McPartlin, J. W. Lauher, *Chem. Eur. J.* **2001**, *7*, 2563.

[9] S. Bellemin-Laponnaz, L. H. Gade, *Chem. Commun.* **2002**, 1286.

[10] S. Bellemin-Laponnaz, L. H. Gade, *Angew. Chem.* **2002**, *114*, 3623; *Angew. Chem. Int. Ed.* **2002**, *41*, 3473.

[11] C. Dro, S. Bellemin-Laponnaz, R. Welter, L. H. Gade, *Angew. Chem.* **2004**, *116*, 4579; *Angew. Chem. Int. Ed.* **2004**, *43*, 4479.

[12] a) B. D. Ward, S. Bellemin-Laponnaz, L. H. Gade, *Angew. Chem.* **2005**, *117*, 1696; *Angew. Chem. Int. Ed.* **2005**, *44*, 1668; b) L. Lukesova, B. D. Ward, S. Bellemin-Laponnaz, H. Wadepohl, L. H. Gade, unpublished results.

[13] C. Foltz, B. Stecker, G. Marconi, H. Wadepohl, S. Bellemin-Laponnaz, L. H. Gade, *Chem. Commun.* **2005**, 5115.

[14] J. A. Takacs, P. M. Hrvatin, J. M. Atkins, D. S. Reddy, J. L. Clark, *New J. Chem.* **2005**, *29*, 263.

[15] See for comparison: P. J. Heard, D. A. Tocher, *J. Chem. Soc. Dalton Trans.* **1998**, 2169.

[16] R. J. Deeth, *Comprehensive Coordination Chemistry II, Vol. 2*, Pergamon Press, Oxford, **2004**.

[17] For examples see: a) S. Hajela, W. P. Schaefer, J. E. Bercaw, *J. Organomet. Chem.* **1997**, *532*, 45; b) C. S. Tredget, S. C. Lawrence, B. D. Ward, R. G. Howe, A. R. Cowley, P. Mountford, *Organometallics* **2005**, *24*, 3136.

[18] M. V. Twigg, J. Burgess, *Comprehensive Coordination Chemistry II, Vol. 5*, Pergamon Press, Oxford, **2004**, p. 403.

[19] See for example: a) H. B. Ammar, J. Le Notre, M. Salem, M. T. Kaddachi, L. Toupet, J. -L. Renaud, C. Bruneau, P. H. Dixneuf, *Eur. J. Inorg. Chem.* **2003**, 4055; b) C. G. Arena, S. Calamia, F. Faraone, C. Graiff, A. Tiripicchio, *J. Chem. Soc. Dalton Trans.* **2000**, 3149.

[20] L. H. Gade, *Koordinationschemie*, Wiley-VCH, Weinheim, **1998**.

[21] a) C. Bianchini, A. Meli, M. Peruzzini, F. Vizza, F. Zanobini, *Coord. Chem. Rev.* **1992**, *120*, 193; b) H. A. Mayer, W. C. Kaska, *Chem. Rev.* **1994**, *94*, 1239; c) C. Bianchini, D. G. Burnaby, J. Evans, P. Frediani, A. Meli, W. Oberhauser, R. Psaro, L. Sordelli, F. Vizza, *J. Am. Chem. Soc.* **1999**, *121*, 5961; d) C. Bianchini, V. Dal Santo, A. Meli, W. Oberhauser, R. Psaro, F. Vizza, *Organometallics* **2000**, *19*, 2433; e) P. Schober, G. Huttner, L. Zsolnai, A. Jacobi, *J. Organomet. Chem.* **1998**, *571*, 279; f) C. Bianchini, M. Frediani, F. Vizza, *Chem. Commun.* **2001**, 479; g) C. Bianchini, M. Frediani, G. Mantovani, F. Vizza, *Organometallics* **2001**, *20*, 2660; h) R. A. Findeis, L. H. Gade, *Eur. J. Inorg. Chem.* **2003**, 99.

[22] J. A. Casares, P. Espinet, J. M. Martin-Alvarez, G. Espino, M. Pérez-Manrique, F. Vattier, *Eur. J. Inorg. Chem.* **2001**, 289.

[23] M. A. Esteruelas, L. A. O. C. A. Apreda, C. Foces-Foces, F. H. C. M. Claramunt, C. L. Elguero, M. Begtrup, *J. Organomet. Chem.* **1988**, *344*, 93.

[24] S. Trofimenko, *Chem. Rev.* **1993**, *93*, 943.

[25] D. Schott, P. S. Pregosin, *Organometallics* **2006**, *25*, 1749.

[26] a) F. H. Allen, O. Kennard, *Chemical Design Automation News*, **1993**, *8*, 1 and 31; b) D. A. Fletcher, R. F. McMeeking, D. J. Parkin, *J. Chem. Inf. Comput. Sci.* **1996**, *36*, 746.

[27] C. Foltz, S. Bellemin-Laponnaz, H. Wadepohl, L. H. Gade, unpublished results.

[28] C. Foltz, G. Marconi, H. Wadepohl, S. Bellemin-Laponnaz, L. H. Gade, unpublished results.

[29] The trisox ligands in the dimers are eclipsed (whereas they are staggered in the mononuclear complexes). This explains the greater stability of the *SSS-SSS* isomer, since the complementary orientation of the isopropyl substituents causes all three isopropyl groups to be totally eclipsed in the *RRR-SSS* complex, whereas they are only partially eclipsed in the *SSS-SSS* complex. Unsurprisingly, these systems were too complex for a successful DFT/ONIOM study. However zinc analogues of the *RRR-SSS* and *SSS-SSS* complexes were computed by using ONIOM (QM/MM) methods, which confirmed the structural validity of the MM calculations.

[30] a) Z. Janas, P. Sobota, T. Lis, *J. Chem. Soc. Dalton Trans.* **1991**, 2429; b) Z. Janas, T. Lis, P. Sobota, *Polyhedron* **1992**, *11*, 3019.

[31] a) U. Bossek, D. Nühlen, E. Bill, T. Glaser, C. Krebs, T. Weyhermüller, K. Wieghardt, M. Lengen, A. X. Trautwein, *Inorg. Chem.* **1997**, *36*, 2834.

[32] Gerd. N. LaMar, *NMR of Paramagnetic Molecules*, Academic Press, New York, **1973**.

[33] a) O. Kahn, *Molecular Magnetism*, Wiley-VCH New York, **1993**; b) R. L. Carlin, *Magnetochemistry*, Springer, Heidelberg, **1986**.

[34] Selected references: a) R. D. Willett, J. A. Haugen, J. Lebsack, J. Morrey, *Inorg. Chem.* **1974**, *13*, 2510; b) R. G. McDonald, M. J. Riley, M. A. Hitchman, *Inorg. Chem.* **1988**, *27*, 894; c) E. I. Solomon, *Comments Inorg. Chem.* **1984**, *3*, 385; d) I. B. Bersuker, *Chem. Rev.* **2001**, *101*, 1067.

[35] J. Zhou, Y. Tang, *Chem. Soc. Rev.* 2005, ***34***, 664.

[36] $[Mo(CO)_3(NCMe)_3]$ was generated in situ by heating $[Mo(CO)_6]$ in acetonitrile. See also: M. D. Curtis, M. S. Hay, *Inorg. Synth.* **1990**, *28*, 150.

[37] L. E. Manzer, *Inorg. Synth.* **1982**, *21*, 135.

[38] M. A. Bennett, A. K. Smith, *J. Chem. Soc. Dalton Trans.* **1974**, 233.

[39] T. G. Schenck, J. M. Downes, C. R. C. Milne, P. B. MacKenzie, H. Boucher, J. Whelan, B. Bosnich, *Inorg. Chem.* **1985**, *24*, 2334.

[40] A. Winzer, E. Born, *Z. Chem.*, **1970**, *10*, 438.

[41] J. J. Borràs-Almenar, J. M. Clemente-Juan, E. Coronado, B. Tsukerblat; MAGPACK; Universidad de Valencia, Valencia, Spain, **1999**.

[42] OpenMoleN, Interactive Structure Solution, Nonius, Delft, **1997**.

[43] G. M. Sheldrick, SHELXS-86, University of Göttingen: Göttingen, Germany, **1986**.

[44] G. M. Sheldrick, SHELXL-97, University of Göttingen: Göttingen, Germany, **1997**.

[45] D. J. Watkin, C. K. Prout, J. R. Carruthers, P. W. Betteridge, R. I. Cooper, *CRYSTALS*, issue 11, Chemical Crystallography Laboratory, Oxford, UK, **2001**.

[46] A. L. Spek, *J. Appl. Crystallogr.* **2003**, *36*, 7.

[47] Gaussian 03, Revision B.03, M. J. Frisch, G. W. Trucks, H. B. Schlegel, G. E. Scuseria, M. A. Robb, J. R. Cheeseman, J. A. Montgomery, Jr., T. Vreven, K. N. Kudin, J. C. Burant, J. M. Millam, S. S. Iyengar, J. Tomasi, V. Barone, B. Mennucci, M. Cossi, G. Scalmani, N. Rega, G. A. Petersson, H. Nakatsuji, M. Hada, M. Ehara, K. Toyota, R. Fukuda, J. Hasegawa, M. Ishida, T. Nakajima, Y. Honda, O. Kitao, H. Nakai, M. Klene, X. Li, J. E. Knox, H. P. Hratchian, J. B. Cross, V. Bakken, C. Adamo, J. Jaramillo, R. Gomperts, R. E. Stratmann, O. Yazyev, A. J. Austin, R. Cammi, C. Pomelli, J. W. Ochterski, P. Y. Ayala, K. Morokuma, G. A. Voth, P. Salvador, J. J. Dannenberg, V. G. Zakrzewski, S. Dapprich, A. D. Daniels, M. C. Strain, O. Farkas, D. K. Malick, A. D. Rabuck, K. Raghavachari, J. B. Foresman, J. V. Ortiz, Q. Cui, A. G. Baboul, S. Clifford, J. Cioslowski, B. B. Stefanov, G. Liu, A. Liashenko, P. Piskorz, I. Komaromi, R. L. Martin, D. J. Fox, T. Keith, M. A. Al-Laham, C. Y. Peng, A. Nanayakkara, M. Challacombe, P. M. W. Gill, B. Johnson, W. Chen, M. W. Wong, C. Gonzalez, J. A. Pople, Gaussian, Inc., Wallingford CT, **2004**.

Received: November 17, 2006
Published online: February 15, 2007

